Response to Anonymous Referee #1

RC = Referee Comment
AR = Author Response

RC: This is an exceptionally thorough and robust modelling-based paper investigating the climate mass balance (CMB), which includes surface and subsurface processes, across Svalbard between 1957 and 2018. It builds on previous similar work by the team, esp. first-authored papers by van Pelt, but this is the first time the latest version of the model (which now includes an improved subsurface scheme based on Marchenko et al., 2017b) has been applied to the whole of Svalbard. The model has a 1 km grid and is run at a 3 hourly time step and is therefore impressive in terms of its spatial and temporal resolution. The CMB is driven by downscaled climate data from the High Resolution Limited Area Model (HIRLAM) regional climate model, which is forced by European Centre for Medium Range Weather Forecasts (ECMWF) reanalyses. This generates the meteorological forcing fields of air temperature, precipitation, cloud cover, relative humidity and air pressure. The work uses an extensive data set of measurements to calibrate / validate the model (mass balance stake measurements from 8 glaciers; weather station data from 6 sites(4 on glacier; 2 off glacier); and shallow ice cores from 4 sites). These are listed in Table 1.The calibration procedure is clearly explained and is logical and the principles have been discussed in two previous referenced papers. Here, parameters that are known to be sensitive are calibrated in sequence as described in section 3.2: 1. Two parameters affecting albedo are calibrated against net SW radiation data; 2. Two parameters in a function describing the downscaling of precipitation are calibrated against winter stake bass balance data; 3. Two parameters affecting summer melt are calibrated with observed summer balance data. The fact that this model has a good history of being used in Svalbard and the fact that the RMSEs and biases after calibration are small, mean that the results will be the best that are currently available. Results presented are quite extensive and informative and, as the authors state in the abstract, should be of value for scientists and practitioners interested in runoff to the oceans as well as ecologists interested in, for example, snow extent, duration and character (which has implications for reindeer grazing, for example).The results / discussion section is focused around a sequence of Figures showing: i)maps of mean conditions across Svalbard; ii) maps of trends over time (where significant); iii) time-series of spatially averaged trends in conditions. The consistency in the way the data are presented make the paper especially useful. The following results are shown and discussed: i) glacier CMB (Fig 5); ii) glacier ELA (Fig 6); iii) glacier firn pore space in top 14 m (Fig 7a,b); iv) firn temperatures at 14 m (Fig 7 c,d); v) refreezing on and off glaciers (Fig. 9); vi) snow onset and disappearance dates off glaciers and across glacier ablation areas (Fig 10); vii) glacier and land runoff. This represents a particularly impressive range of data sets presented and discussed from this type of modelling study. The paper discusses sources of uncertainty throughout and has a synthesis section on this towards the end (section 4.6). Where results differ from those of similar previous work (but using earlier versions of the model, calibrated in different ways, run over different time periods, and across different spatial domains) the magnitudes and reasons for the discrepancies are revealed. The results and implications of the Svalbard work are also discussed in the context of similar work where appropriate in Arctic Canada and Greenland; this is especially the case when discussing the important finding of decreasing refreezing rates over time and therefore an increase in the likelihood of firn aquifers developing around the ELA. So overall this represents excellent work by this team and shows the value of long-term monitoring but also the collection of shorter-term field measurements and their rigorous use in model development and application. The work is exceptionally well presented in terms of the overall paper structure, as well as the clarity and precision of the writing, but also in the consistency and quality of the Figures.

AR: We are very grateful for this very positive feedback! And we thank the reviewer for the useful comments, which we address below, and which have helped to improve the manuscript.

RC: As mentioned above, quoting from the paper, the meteorological forcing fields used to drive the CMB model are: air temperature, precipitation, cloud cover, relative humidity and air pressure. The answer is probably elsewhere in previous papers but a brief note on how these are used (together with other fields I assume) to calculate energy/ mass balance at the surface would be useful. For example, there is no mention of wind-speed here, and yet I assume this is required together with air temp and relative humidity to calculate the turbulent fluxes? And I assume theoretical clear sky solar radiation is used together with cloud cover to determine the incoming SW radiation?

AR: More details on the individual energy balance components and their dependence on climate fields is given in Van Pelt et al. (2012). However, we agree some more information would be helpful to include here as well, so we added the following in Sect. 3.1:

"Solving the surface energy balance requires input of near-surface meteorological conditions, including air temperature, cloudiness, relative humidity, air pressure and precipitation (Van Pelt et al. 2012). No wind information is needed since sensible and latent heat exchange depend solely on near-surface temperature and specific humidity gradients, following katabatic turbulent exchange relations by Oerlemans & Grisogono (2002)."

RC: P8 L17-19. The Bougamont et al (2015) work is for Greenland. How do you know that parameter values derived for the GrIS for t* are valid on Svalbard. The final sentence refers to the work on the GrIS I assume. Given the importance of albedo for melt and mass balance etc, some clarity is needed here about the validity of using the parameter values relevant for GrIS here in Svalbard. Is this a source of uncertainty that needs better recognition?

AR: This a good point. At present we cannot confirm or deny that the t* values from Bougamont et al. (2005) are appropriate for Svalbard glaciers. Although we did not calibrate t* values, it is worth mentioning that as part of the calibration procedure in Section 3.2 we have used SW net observations from three AWSs in Svalbard to calibrate fresh snow albedo and the minimum snowfall amount at which the snow albedo is reset to the fresh snow albedo. These are two albedo parameters to which modelled melt has in a previous study (Van Pelt et al. 2012) been shown to be highly sensitive. By using SWnet data in the calibration, we avoid substantial biases in the surface energy balance (and calculated melt rates) resulting from potentially inaccurate parameter values affecting incoming and reflected SW radiation, including t*. However, any inaccuracies in chosen values of, for example, t* would be compensated for by a potentially different value for the fresh snow albedo and/or the snowfall threshold. In future work, a more detailed comparison of modelled and observed albedo at multiple sites in Svalbard and for longer time-series would allow for more extensive calibration of albedo parameters. To acknowledge uncertainty in parameters like t*, we now include the following sentences in Sect. 4.6:

"Energy balance parameters were taken as in the aforementioned studies, with the exception of the fresh snow albedo (α_{fs}), the associated minimum snowfall threshold (P_{th}), and the background turbulent exchange coefficient (C_b), which were calibrated against observational data (Sect. 3.2). The new albedo scheme assumes that previously used values of t for Greenland (Bougamont et al. 2005) are also applicable to Svalbard. Potential inaccuracies in parameters like t* will introduce uncertainty in modeled albedo values, as it introduces compensating errors in calibrated parameters; in the case of t*, compensating errors would arise in α_{fs} and P_{th}. However, the calibration procedure assures that, despite compensating errors, net biases in relevant model output, e.g. melt, is minimized. More careful calibration of albedo parameters, including t*, is planned for future work using a more extensive dataset of albedo measurements across Svalbard."*

Also, in response to reviewer #2, we have additionally extended the description of albedo in Sect. 3.1, to better introduce the albedo scheme and give more information on where the parameter values come from (if not calibrated).

RC: P9 L33&34. It's stated that the parameter Tsr has a strong impact on summer melt but most previous work has shown it's particularly important for winter accumulation. I can see it'll have an indirect impact on summer melt because of its direct impact on winter accumulation. Can you better justify why this parameter is tuned to the summer mass balance data and not the winter mass balance data?

AR: Indeed, Tsr has some impact on winter balance as well. However, we find that the sensitivity of the winter balance to Tsr changes is about twenty (!) times smaller than the sensitivity of summer balance to Tsr changes for the mass balance stake locations. Several factors play a role here, but the relatively insensitivity of winter balance to Tsr is primarily explained by the fact that rainfall during the core winter season is (still) rare in Svalbard, especially at higher elevations. And in case any rain falls during the core winter season, most of the rain water will refreeze in the snow pack thereby not inducing any runoff. The significant impact of Tsr on melt and runoff (and thereby summer balance) has previously been quantified in Van Pelt et al. (2012) for Nordenskiöldbreen. We have added a sentence to Sect. 3.2 explaining the relative insensitivity of winter balance to Tsr.

RC: P22 L1-2. There is a bit of confusion here as you seem to be discussing runoff rates due only to snow melt on land and comparing them to runoff rates due to snow and ice melt across glaciers. But, as you say later, runoff from land includes rainfall. Does runoff from glaciers also include rainfall? A better articulation of precisely how runoff is calculated for land and for glaciers is needed before the two values are compared. Can you separate out runoff from snow(ice) melt from runoff due to rainfall?

AR: We now try to avoid this confusion by first giving the definition of runoff in Sect. 4.5:

"Here, runoff refers to the amount of water originating from melt and rainfall at the surface and available at the base of the snow/firn pack (if present) or ice/soil surface after accounting for retention by refreezing and irreducible water storage."

Typos / technical issues

RC: Abstract P1 L4. Could say: "climatic mass balance (CMB) for the glaciers, snow conditions and runoff"
RC: L8. Suggest "small" not "weak"
RC: P2 L4. "reveals" not "reveal"? The Longyearbyen time-series is singular not plural?
RC: P2 L19. Could add the following reference to this list of previous studies here:
Rye, C.J., Willis, I.C., Arnold, N.S. and Kohler, J., 2012. On the need for automated multiobjective optimization and uncertainty estimation of glacier mass balance models. Journal of Geophysical Research: Earth Surface, v. 117,
RC: P4 L21 "altitudes" (i.e. plural)

AR: All fixed.

RC: P5 Table 1. Table is not quite self-contained. Suggest adding to Table Heading and referring to Fig 1 heading for abbreviation names. Also to explain variables or say they're explained in the text.

AR: We have extended the Table header with more details about the used abbreviations.

RC: P5 L10. Could add ref to Table 1 after final sentence here.
RC: P6 L8 suggest "made" not "done"
RC: P7 L5. Suggesting adding months when end of summer measurements are typically made (like April is stated earlier in the sentence for when Spring measurements are made). I'm guessing this is August or September (since 1 Sept. is stated as an average time below)?
RC: P7 L15 Could delete "above described"

AR: All fixed.

RC: P11 L4 and Table 2. The term 'bias' is introduced here and referred to as "modelled minus observed". There are different definitions of bias so it might be worth clarifying precisely how it's defined here. Is it simply the Mean Absolute Difference (MAD)?

AR: We have added that the bias is the mean absolute difference.

RC: P11 L29. "five" should read 'six" here I assume? There are 6 sites mentioned in Table 1 and 3.
RC: P11 L32. "…temperatures for both…"

AR: Both fixed.

RC: P13 L11. Should this say "net CMB" to distinguish it from winter or summer that are also reported? Could clarify the first time you refer to net CMB, e.g. say "net CMB, hereafter just CMB…" or some such. In Abstract you might then also add the word "net"?

AR: Good point. We have followed these suggestions.

RC: P17 L25-27. There is also some similar work to this reported recently from the Larsen C ice shelf, Antarctica that could also be compared / referenced. e.g.

Hubbard, B., Luckman, A., Ashmore, D.W., Bevan, S., Kulessa, B., Kuipers Munneke, P., Philippe, M., Jansen, D., Booth, A., Sevestre, H., Tison, J.L., O'Leary, M., and Rutt, I., 2016. Massive subsurface ice formed by refreezing of ice-shelf melt ponds. Nature Communications, 7.

Bevan, S. L., Luckman, A., Hubbard, B., Kulessa, B., Ashmore, D., Kuipers Munneke, P., O'Leary, M., Booth, A., Sevestre, H., and McGrath, D. 2017. Centuries of intense surface melt on Larsen C Ice Shelf, The Cryosphere, 11, 2743-2753.

AR: References added.

RC: P20 L3-5. There is a lack of clarity here. Here and the few sentences above need to better distinguish between a discussion of snow onset date and snow disappearance date. There's ambiguity here as it seems as though you might be comparing the trend in onset date (+1.4 days / decade) found in this study with trends in BOTH the onset date AND the disappearance date in a previous study. There is a bigger discrepancy in the disappearance date trends in the two studies than there is between the two onset date trends, and this probably needs stressing and discussing. I wouldn't say a disappearance date trend of +0.7 days / decade is comparable with 0 days per decade.

AR: We have reformulated the associated sentences to improve clarity.

RC: P23 L34. I think this should just read "…simulation, using the climate forcing…".

AR: Fixed.

Response to reviewer #2 (Marco Möller)

RC = Referee Comment
AR = Author Response

RC: Van Pelt et al. present a multi-decadal modeling study regarding snow and glacier mass balance on Svalbard that yielded results on a so-far unprecedented level of detail with respect to model resolution and captured processes. I very much congratulate the authors to this very thoroughly performed, documented and discussed modeling study which provides extremely valuable new knowledge to the field of Svalbard-wide glacier and snow research. I have no severe concerns regarding publication of this article. However, in its present form, the model description lacks a couple of important details that need to be added to the descriptions in order to make the methodology easier to follow. In this respect, three substantial issues need special and more extensive attention, including limited additional data analysis. Taken together, I recommend to accept the manuscript of Van Pelt et al for publication in The Cryosphere after a minor revision along the issues outlined below.

AR: We thank the reviewer for the very positive feedback! We are also grateful for the substantial and detailed comments, which have helped us to improve the manuscript.

Substantial comments:

RC: 1) P4L30f (& P9L16ff): I understand that you first linearly interpolate your 10km HIRLAM precipitation grid to the 1km resolution of your model. So far so good. However, in the next step you describe the application of a fixed linear fractional increase with elevation that you apply in addition. This step causes some concerns. I assume that the 10km elevation information in HIRLAM are not based on the S0 Terrengmodel Svalbard that you use in your mass balance model, right? This means that the average of the 1km elevations in your model across each 10km HIRLAM grid point and the elevation of this HIRLAM grid point itself do not equal each other. If this is the case, it introduces a physical inconsistency. Depending on the area altitude distribution of the 1km model grid points within each 10km HIRLAM grid point you either increase or decrease the total amount of precipitation that falls within this grid point by applying a fixed linear precipitation increase. Hence, the precipitation amounts which had been modeled by HIRLAM in a way that is physically consistent to synoptic forcing, are altered completely by your downscaling scheme. Moreover, this happens completely unstructured with respect to space, as the degree of alteration is only determined by the differences between the means of the 1km model elevations and the 10km HIRLAM elevations. I'm not sure if my interpretation above is what really happens; it could have also been a simple misunderstanding of your descriptions. In any case, I'd suggest that you comment on this issue in detail in the uncertainty discussion and/or revise your descriptions in the methods section accordingly to make them unambiguous in this respect.

AR: We believe we understand the reviewer's concern, but do not regard the precipitation - elevation correction method as physically inconsistent. The two reasons to apply the precipitation – elevation equation are to 1) account for any elevation differences between the detailed 1-km DEM and the coarser 10-km HIRLAM DEM (interpolated to 1-km resolution), and 2) to correct for any Svalbard-wide biases between modelled and observed precipitation. The former is controlled by K2, while the latter is controlled by K1. This precipitation adjustment is not 'mass-conserving', since we correct for biases between model and observations (K1 is not equal to 1). Furthermore, as suggested by the reviewer, there may be (small) elevation deviations between the mean of 1-km height values and the corresponding regional climate model elevation value. This is not at all problematic, since we in fact desire that our correction method also compensates for these height errors by altering the precipitation amount. The actual 1-km DEM will contain more detail than the interpolated HIRLAM-DEM; any positive deviation of the surface height will lead to a positive correction of the local precipitation, while a negative height deviation will lead to a negative precipitation correction. The main advantage of this downscaling is that we introduce the effect of orographic lifting on precipitation at scales

smaller than the 10-km spatial resolution of the regional climate model. To clarify our approach, we have added the following in Sect. 3.2:

"Values from the 1-km DEM (z) will contain more detail than the z0 values interpolated from the coarser regional climate model grid; any positive deviation of the surface height (z-z0>0) will lead to a positive correction of the local precipitation, while a negative height deviation (z-z0<0) will lead to a negative precipitation correction. With this approach, we account for the effect of local topography on precipitation, thereby capturing the impact of orographic lifting at scales smaller than the resolution of the regional climate model. In addition to compensation for biases in modelled precipitation (by calibrating K_1) potential surface height discrepancies at spatial scales of 10-km and greater that may arise from the use of a different DEM in the regional climate model are also automatically compensated for.

RC: 2) P8L11ff: You implemented two novelties in your model. While the first one, the physically based percolation scheme, is fully referenced, the second one is not. How were the parameters of your newly incorporated albedo scheme chosen? If you use a new or updated scheme, then you need to include information about how it was calibrated or how it is justified from a physical point of view. As you have various AWS data available, I suppose that you could easily validate your new albedo scheme with shortwave radiation measurements from these stations. I do not ask for including an additional figure on this (even if it would be nice to have), but at least you should provide some comparative albedo numbers to validate the novelty in your model, especially its ability to produce a reliable course over the year. Your Svalbard-wide distribution of albedo values may also be compared to those modeled and described for 1979-2015 by Möller & Möller (2017) on the basis of MODIS data. This would yield important insights into the reliability of your so-far unreferenced albedo scheme.

AR: This is a valid point. A similar comment was given by reviewer #1, who questioned the transferability of albedo parameters (t*) from Greenland to Svalbard. We agree that some more information about the albedo scheme is needed. In Sect. 3.1, we have now extended the description of the albedo scheme by explaining what parameter values were chosen and based on which references. First of all, we refer to Bougamont et al. (2005) for the characteristic decay time-scale (t*) values, which were optimized on Greenland and used here as well. In the uncertainty discussion (Sect. 4.6), we have now added a discussion on uncertainty related to the potential errors in chosen albedo parameter values like t* (in response to reviewer #1). Secondly, for three other albedo parameters (albedo of ice [0.39], albedo of firn [0.52] and characteristic snow depth [7 mm w.e.]) we used values that have been calibrated in a previous study with the model (Van Pelt and Kohler, 2015). This information is now added to Sect. 3.1. Thirdly, regarding calibration/validation of the new albedo scheme, it is worth mentioning that we optimize two key albedo parameters (fresh snow albedo & snowfall threshold to reset albedo to the fresh snow albedo) against observations of net SW radiation (see Sect. 3.2). By doing so any biases in net SW radiation resulting from the new albedo scheme are minimized. A sentence has been added to Sect. 3.1 to clarify this. We do not think it is needed to include a more detailed validation or comparison of albedo time-series in this study, although it would be useful to do this in future work with a more specific focus on albedo (this is now also discussed in Sect. 4.6).

The new description of albedo in Sect. 3.1 reads:

"Additionally, we have extended the original snow age and snow depth dependent albedo scheme (Oerlemans et al. 1998). The original fixed characteristic time-scale for exponential decay of snow albedo due to ageing has been replaced with a temperature dependent time-scale (t). As in Bougamont et al. (2005) snow albedo decays fastest when the surface is melting (t* = 15 d), and for dry snow t* linearly increases from 30 to 100 days between 0 and -10 oC. The updated albedo scheme avoids overestimation of the albedo of melting surfaces in the early melt season. Other albedo parameters, including the albedo of ice (0.39), albedo of firn (0.52), and the characteristic snow depth for albedo decay of thin snow covers (7 mm w.e.) were taken as in (Van Pelt and Kohler, 2015). To avoid potential systematic biases resulting from the new albedo scheme, we have included the*

fresh snow albedo (α_{fs}) minimum snowfall threshold used to reset the snow albedo to the fresh snow albedo (P_{th}) in the calibration process, as described in Sect. 3.2."

The new discussion about uncertainty in albedo parameters in Sect. 4.6 reads:

"*Energy balance parameters were taken as in the aforementioned studies, with the exception of the fresh snow albedo (α_{fs}), the associated minimum snowfall threshold (P_{th}), and the background turbulent exchange coefficient (C_b), which were calibrated against observational data (Sect. 3.2). The new albedo scheme assumes that previously used values of t* for Greenland (Bougamont et al. 2005) are also applicable to Svalbard. Potential inaccuracies in parameters like t* will introduce uncertainty in modeled albedo values, as it introduces compensating errors in calibrated parameters; in the case of t*, compensating errors would arise in α_{fs} and P_{th}. However, the calibration procedure assures that, despite compensating errors, net biases in relevant model output, e.g. melt and runoff, are minimized. More careful calibration of albedo parameters, including t*, is planned for future work using a more extensive dataset of albedo measurements across Svalbard."*

Regarding the albedo maps that were presented in Möller and Möller (2017) we are happy to share maps with the reviewer (and the data behind them) that can be used for comparison. When writing this manuscript, we have carefully selected the variables that we thought were of most value to present and albedo was in the end not selected. We decided to have more focus on the mass balance components and stay away from a detailed analysis of individual energy balance components, including albedo.

RC: 3) P8L25ff: The application of RMSE minimization for finding the optimum values for K1 and K2 is certainly valid. However, I'd like to point towards a potential problem.
In case the stake readings that are used as reference are not distributed equally with elevation, the RMSE minimization might not yield a proper combination of K1 and K2.
This is because elevations with the highest number of stake readings are overrepresented and the minimization procedure thus concentrates on getting the accumulation at this specific elevation well while paying less attention to the other, underrepresented elevations. This issue has been detailed and documented for stake-based calibrations across Svalbard before by Möller et al. (2016) and you should at least account for it in the text. However, it would be better to check it in detail in order to avoid potentially wrong gradients or scaling coefficients that might lead to substantial under and/ or overestimation of climatic mass balance towards higher elevations. My concern is backed by the fact that the winter balances in Figure 3 clearly show, that modeled values tend to systematically underestimate the measured ones the more positive they become. If you visually place a linear fit to the blue points, the line would have a slope that for sure is distinctly larger than 1. I do not think that this issue will compromise your overall results as it probably only affects the most positive mass balances. Nevertheless, it needs to be presented in the uncertainty discussions section.

AR: This is an interesting comment. We will start our response by showing a figure. To assess whether there may be a potential bias increasing with elevation we have made height profiles of b_w, b_s and b_n for the eight observed glaciers. Here data are averaged in 100 m elevation bins and over the whole observation period.

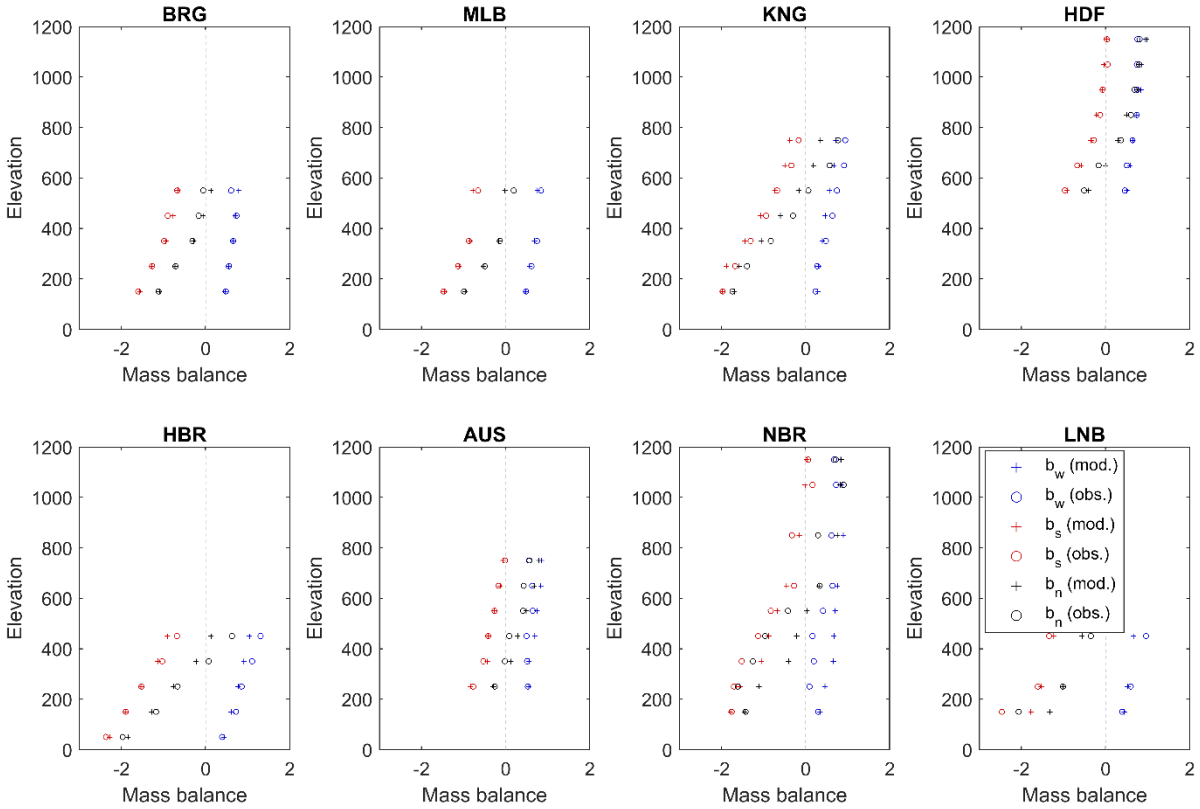

What can be seen is that there are some glaciers (particularly KNG and HBR) where b_w biases indeed increase with elevation. However, for the glaciers with the highest elevations, i.e. over 1000 m a.s.l. (HDF and NBR), we do not see this effect. What this shows is that the bias for high observed b_w values that seems apparent in Fig. 3 in the manuscript is likely to come from underestimated precipitation at the highest stakes on KNG and HBR, where long data records exist (i.e. many data points) and precipitation amounts are among the highest on Svalbard (much higher than at the much higher-located stakes on NBR and HDF). These local effects are apparently not properly captured by the model, but it cannot be concluded that precipitation amounts are off at high elevations in general. We now refer to Möller et al. (2016) and have extended the discussion on this at the end of Sect 3.2:

"On the other hand, underestimation of b_w is apparent for KNG and HBR (Fig. 3, Table 2), which results from underestimated orographic precipitation at high elevations on these glaciers. Nevertheless, high-elevation biases of b_w do not arise on the only two glaciers extending above 1000 m a.s.l., which indicates that the b_w offsets on KNG and HBR are not a systematic feature for high elevation sites in general. The relative lack of stake observations at heights above 1000 m a.s.l. implies increased uncertainty of modelled precipitation estimates at these elevations (Möller et al. 2016)".

Detailed comments:

RC: P2L19f: The reference to Day et al. (2012) is misleading here. They only calculate changes in surface mass balance on the basis of seasonal sensitivity characteristics. They neither use a mass balance model nor do they calculate absolute Svalbard wide mass balance numbers. Instead of Day et al. and to complete the ensemble of Svalbard-wide mass balance calculations a reference to Möller et al. (2016) is missing here.

AR: We have added a reference to Möller et al. (2016) and removed the reference to Day et al. (2012).

RC: P2L34f: The references to Hagen et al. (2003) and Winther et al. (2003) are completely outdated as numerous studies related to seasonal snow coverage on Svalbard have been published since then, partly even with contributions of one or several co-authors of this study here. Hence, there is a need to include more up-to-date references here (e.g. Grabiec et al. 2011 or else).

AR: We believe the two 2003 references are still relevant, but now also include the suggested newer reference to Grabiec et al. (2011).

RC: P4L27: Include information about which ECMWF reanalysis products are used and over which periods. Even if this is partly deducible from the references it needs to be explicitly stated in the text.

AR: Fixed.

RC: P4L30f: Far more, especially quantitative, information about the applied lapse rates, increases and decays is needed here. The reader must fully understand what has been done without digging into previous literature.

AR: This is a good point. We have added the following sentences in Sect. 2.1:

"Elevation functions for temperature and air pressure were constructed per 3h time-step through respectively linear and exponential regression of the regional climate model values and their corresponding elevations; this procedure was repeated for blocks of 4x4 grid cells and regression coefficients were averaged for the whole grid to obtain a single lapse-rate for temperature and exponential decay coefficient for air pressure per time-step."

RC: P5L1: How did you calculate the significance of the trends? Information about this needs to be included here.

AR: It is now added that significance means that a zero trend is not included in the 2-sigma confidence bounds of a trend.

RC: Figure 2: Just out of curiosity (as it is out of the scope of your study): do you have an explanation for the rather interesting pattern of precipitation trends visible in (d). I especially refer to the east coast of Wijdefjorden here.

AR: Well, the precipitation trends are generally very small; the trend values that still appear as colors (non-gray) in the map are also only just significant. In general a slight precipitation increase in Svalbard has also been observed in observational records (see also Introduction). And the somewhat stronger precipitation trends in northern Svalbard could be a result of retreating sea ice having a larger impact on moisture availability there. This effect has also been suggested to amplify in a future climate (see for example the recent Climate in Svalbard 2100 report).

RC: P7L8: This value seems to be reasonable as it is quite often used for the transition from snow to firn. However, the choice appears to be rather arbitrary in the present form of the text. Information about how this choice was made, including appropriate reference, needs to be given here. Moreover, as you give explicit information about the density applied to remaining snow you should also do so for other snow cover to ablation conversions that you consider in your model.

AR: We have removed the 550 kg m^{-3} value from the paper and instead refer to Van Pelt et al. (2018) where the summer balance calculation from stake measurements (in that case on Nordenskiöldbreen) is also described. For the conversion of stake heights to winter balance estimates, fresh snow density is needed, which is based on snow pit data. Since this is already described in Van Pelt et al. (2016) we only keep the reference to that paper for more information.

RC: Figure 5b: One might think about the color scale here. People tend to associate blue colors with cooler conditions, which means more positive mass balances in glaciological studies. However, in the

current version of this figure, blue represents a negative trend and thus a development towards more negative mass balances. Maybe it would be better skip the in the first instance ambiguous blue-red color scale here in favor of something more "uncommon". But that's just a suggestion as it reflects a rather subjective view.
RC: Figure 10: Same "problem" with the color scale as in Figure 5b. But this is still only a suggestion.

AR: Thanks for the suggestion. We understand the confusion this may cause, but we still think it is good to stick to the current choice of colormap for the sake of consistency. We like to be consistent throughout the manuscript with blue colors for a negative trend and red colors for a positive trend. For some variables this may be intuitive (e.g. temperature), whereas for others like CMB it may be counterintuitive, but this seems unavoidable.

RC: Figure 9: An additional map showing the distribution of the percentage of melt and rainwater that is refrozen should be added here and any inferable information should to be included in the discussion where appropriate.

AR: This is a useful suggestion, and we have decided to add two panels to Fig. 9 showing the fraction of melt and rainfall that refreezes (Fig. 9c) and the associated trends (Fig. 9d). These new results interestingly show that highest refrozen fraction values occur on Lomonosovfonna and lowest values in coastal regions in southern Svalbard. Furthermore, it is found that no sites experience a refrozen fraction that is close to 1 (values up to 0.8 are found), which indirectly shows the absence of cold firn in Svalbard during the simulation period. Trends of the refrozen fraction reveal most negative values in northern Svalbard. All this is now discussed in more detail in the second and third paragraph in Sect. 4.3.

RC: P22L21ff: You describe the usage of a fixed DEM and fixed glacier mask as a potential source of uncertainty and error. However, in the beginning of your paper you explicitly state that you calculate reference surface balances. Hence, your results do not suffer any "uncertainties" or "errors" due to the usage of fixed glacier extents and elevations.
They simply represent a completely different quantity that is not comparable to "real" climatic mass balances which would be based on a time-varying glacier topography. This needs to be made clear in this section. You could of course keep the given descriptions, but treat them as deviations to what really happened on the glaciers and not as "uncertainties".

AR: Good point. We now refer to 'deviations' rather than 'uncertainties' instead, and have added some text on the use of "reference" surfaces for mass balance modelling (Sect. 4.6).

RC: P23L7ff: The discussion of misestimations of precipitation fits to my substantial comment 3) in the beginning. The issue raised in this substantial comment needs to be included in this discussion, too.

AR: We have added some discussion on this now earlier on in Sect. 3.2. For more details, see our reply to substantial comment 3).

RC: P23L17ff: You might explicitly refer to the influences of wind-drifted snow, i.e. its potential to systematically increase or decrease local as well as regional accumulation rates.
This information is certainly assumed in the sentence in question here, but it should be explicitly stated and referenced (e.g. Jaedicke and Gauer 2005; Grabiec et al. 2011).

AR: We have added a notion on wind-driven snow redistribution and included the additional references (Sect. 4.6).

A long-term dataset of climatic mass balance, snow conditions and runoff in Svalbard (1957-2018)

Ward van Pelt[1], Veijo Pohjola[1], Rickard Pettersson[1], Sergey Marchenko[1], Jack Kohler[2], Bartek Luks[3], Jon Ove Hagen[4], Thomas V. Schuler[4,5], Thorben Dunse[4,6], Brice Noël[7], and Carleen Reijmer[7]

[1]Department of Earth Sciences, Uppsala University, Uppsala, Sweden
[2]Norwegian Polar Institute, Tromsø, Norway
[3]Institute of Geophysics, Polish Academy of Sciences, Warszawa, Poland
[4]Department of Geosciences, University of Oslo, Oslo, Norway
[5]Department of Arctic Geophysics, University Centre in Svalbard, Longyearbyen, Svalbard
[6]Department of Environmental Sciences, Western Norway University of Applied Sciences, Norway
[7]Institute for Marine and Atmospheric Research Utrecht, Utrecht University, Utrecht, The Netherlands

Correspondence: Ward van Pelt (ward.van.pelt@geo.uu.se)

Abstract. The climate in Svalbard is undergoing amplified change compared to the global mean. This has major implications for runoff from glaciers and seasonal snow on land. We use a coupled energy balance − subsurface model, forced with downscaled regional climate model fields, and apply it to both glacier-covered and land areas in Svalbard. This generates a long-term (1957-2018) distributed dataset of climatic mass balance (CMB) for the glaciers, snow conditions and runoff with a 1×1-km spatial and 3-hourly temporal resolution. Observational data including stake measurements, automatic weather station data and subsurface data across Svalbard are used for model calibration and validation. We find a weakly positive mean net CMB (+0.09 m w.e. a^{-1}) over the simulation period, which only fractionally compensates for mass loss through calving. Pronounced warming and a ~~weak~~ small precipitation increase lead to a spatial-mean negative net CMB trend (-0.06 m w.e. a^{-1} $decade^{-1}$), and an increase in the equilibrium line altitude (ELA) by 17 m $decade^{-1}$, with largest changes in southern and central Svalbard. The retreating ELA in turn causes firn air volume to decrease by 4% $decade^{-1}$, which, in combination with winter warming induces a substantial reduction of refreezing in both glacier-covered and land areas (average -4% $decade^{-1}$). A combination of increased melt and reduced refreezing cause glacier runoff (average 34.3 Gt a^{-1}) to double over the simulation period, while discharge from land (average 10.6 Gt a^{-1}) remains nearly unchanged. As a result, the relative contribution of land runoff to total runoff drops from 30 to 20% during 1957-2018. Seasonal snow on land and in glacier ablation zones is found to arrive later in autumn (+1.4 days $decade^{-1}$), while no significant changes occurred in the date of snow disappearance in spring/summer. Altogether, the output of the simulation provides an extensive dataset that may be of use in a wide range of applications ranging from runoff modelling to ecosystem studies.

1 Introduction

The Arctic climate is changing at a faster rate than the global mean (IPCC, 2014; AMAP, 2017) as a result of climate feedbacks triggered by changing sea-ice cover (Serreze and Barry, 2011; Bintanja and Van Der Linden, 2013). The climate in Svalbard,

located at the southwestern boundary of wintertime sea-ice and at the northeastern end of the North Atlantic Drift, is primarily controlled by sea-ice cover trends (Divine and Dick, 2006; Day et al., 2012) and trends in prevailing wind direction (Hanssen-Bauer and Førland, 1998; Lang et al., 2015). The homogenized observational air temperature time-series from Longyearbyen (1898−2012) ~~reveal~~ reveals a linear trend of 2.6 ^{o}C per century, with three−four times stronger warming in winter/spring than in summer (Nordli et al., 2014). Longterm precipitation records in Svalbard are uncertain due to the local character of measurements and instrumental errors (Førland and Hanssen-Bauer, 2000; Førland et al., 2011), but show an overall increase that is coherent with large-scale Arctic-wide assessments (e.g., Zhang et al., 2013). Ongoing climate trends strongly affect the state of both glaciers and seasonal snow in Svalbard (e.g., Van Pelt et al., 2016a; Østby et al., 2017).

In response to warming, glaciers in Svalbard with a current estimated volume of ∼6,200 km^3 (1.5 cm sea level equivalent; Fürst et al., 2018), and area of 33,775 km^2 ($\sim 57\%$ of the total area of Svalbard; Fig. 1), have in recent decades shrunk by ~ 80 km^2 a^{-1} (Nuth et al., 2013), primarily due to low-elevation thinning and associated retreat (e.g., Moholdt et al., 2010; Nuth et al., 2012). Total glacier mass balance is the sum of frontal ablation, basal ablation, and the climatic mass balance (CMB), representing the mass change due to atmosphere - surface - snow pack interactions (Cogley et al., 2011). CMB measurements in Svalbard started on Austre Brøggerbreen (since 1967), followed by Midtre Lovénbreen (since 1968), both in northwestern Svalbard. Since the 1980s, CMB monitoring has extended also to southern, central and northeastern Svalbard (Fig. 1, Table 1). Although a negative trend in CMB is apparent for most observed glaciers, the scarcity of the data in space and time does not allow for a detailed estimation of long-term CMB trends for different regions in Svalbard. To overcome this, CMB models, commonly forced with regional climate model or reanalysis fields, have previously been applied to individual glacier basins ~~(e.g., Möller et al., 2013; Van Pelt et al., 2012; Van Pelt and Kohler, 2015)~~ (e.g., Rye et al., 2012; Van Pelt et al., 2012; Möller et al., 2013 well as for all glaciers in Svalbard ~~(e.g., Day et al., 2012; Lang et al., 2015; Aas et al., 2016; Østby et al., 2017; Möller and Kohler, 2018)~~(e The use of different CMB models, climate forcings, model calibration and spatial resolution has resulted in a relatively large spread of multi-decadal Svalbard-wide mean CMB and trends in CMB in available literature. For example, Lang et al. (2015) report a negligible CMB trend for 1979−2013, while Østby et al. (2017) report a strong CMB decline over the same period and the longer period 1957−2014. As a result, despite confirmed significant warming in Svalbard since the 1960's (Nordli et al., 2014), its impact on glacier CMB remains poorly constrained.

Recent climate warming not only has a major impact on glaciers, but also exerts a strong influence on the state of seasonal snow in the glacier-free parts of Svalbard. Previous work has shown that despite a modest increase in Arctic precipitation in recent decades (Zhang et al., 2013; Bintanja and Selten, 2014), the duration of the snow-free season is increasing and that the area with a permanent snow cover is declining (Van Pelt et al., 2016a). It has also been shown that thick ice layers may form in snowpacks during winters with heavy rainfall events, thereby limiting reindeer access to food supplies and leading to population declines (Kohler and Aanes, 2009; Hansen et al., 2014). Formation of ice at the base of seasonal snowpacks has been projected to increase in a future climate (Hansen et al., 2011), as the fraction of precipitation falling as rain is rising (Bintanja and Andry, 2017). In situ snow observations by means of probing, snow pits, ground-penetrating radar and remote sensing, have been extensively used to assess local-scale patterns and evolution of seasonal snow in Svalbard

Figure 1. Topographic map of Svalbard with different elevation colormaps to distinguish between glacier-covered and land areas. Sites of in situ data collection, including stakes, weather stations and shallow ice cores, are indicated [ABB = Austre Brøggerbreen; AUS = Austfonna; HBR = Hansbreen; HDF = Holtedahlfonna; KNG = Kongsvegen; MLB = Midtre Lovénbreen; LNB = Linnébreen; NBR = Nordenskiöldbreen; LYB = Longyearbyen; NA = Ny-Ålesund]. UTM coordinates in this and later figures are in zone 33 X. The digital elevation model and mask used to produce the map are described in Sect. 2.1, and an overview of the observational data is given in Table 1.

35 ~~(e.g., Hagen et al., 2003; Winther et al., 2003; Van Pelt et al., 2014)~~(e.g., Hagen et al., 2003; Winther et al., 2003; Grabiec et al., 2011; Va
but provide only limited insight in snowpack dynamics at large spatial and temporal scales.

In this study, we use a coupled surface energy balance - multilayer subsurface model (Van Pelt et al., 2012, 2016b) and apply it to all of Svalbard to generate a model dataset with a 3-hourly temporal and 1×1-km spatial resolution for the period 1957−2018. In contrast to previous large-scale coupled modelling of glaciers in Svalbard (Lang et al., 2015; Aas et al., 2016; Østby et al., 2017), we apply our model to both glacierized and glacier-free terrain. Furthermore, we implement improved model physics, and adopt new techniques for climate downscaling and calibration (Sect. 3). Two different model setups are chosen to enable simulating deep subsurface conditions for the glacier-covered part and detailed seasonal snow pack evolution on permafrost for the land part. In situ data of stake mass balance, automatic weather stations and snow conditions (Sect. 2) are used for model calibration and validation (Sect. 3). In Sect. 4 we present and discuss spatial patterns and trends of CMB, snow and firn conditions on glaciers, as well as seasonal snow conditions on land, which allows for a detailed and unprecedented quantification of seasonal snow and glacier contributions to total discharge from the Svalbard archipelago. The output dataset provides crucial input data for further cryospheric analyses, and may serve as input for studies of marine and terrestrial ecosystems.

2 Data

In this section we describe the data used as model input (Sect. 2.1), for model calibration (Sect. 2.2) and for validation of model results (Sect. 2.3). An overview of all observational data used is given in Table 1.

2.1 Input data

A digital elevation model (DEM) with a 20-m spatial resolution, provided by the Norwegian Polar Institute (S0 Terrengmodel Svalbard), has been averaged onto a 1-km resolution grid for the model experiments. Resulting elevations range from sea level to 1552 m a.s.l. (the actual highest point on Svalbard is 1717 m). Glacier outlines were extracted from the GLIMS database (Global Land Ice Measurements from Space; König et al., 2014) and used to split the terrain into land and glacier-covered areas (Fig. 1), and to estimate equilibrium line ~~altitude~~ altitudes for individual glacier basins. Glacier outlines correspond to the period 2001−2010, while the data behind the DEM where collected during 1990−2010. We assume fixed elevations and glacier mask over the simulation period to produce ~~reference~~ surface mass balance and related quantities for a reference surface (Elsberg et al., 2001).

To generate meteorological forcing fields of air temperature, precipitation, cloud cover, relative humidity and air pressure, we use 3-hourly output from the High Resolution Limited Area Model (HIRLAM) regional climate model (NORA10 dataset; Norwegian Meteorological Institute; Reistad et al., 2011), covering the period 1957−2018. HIRLAM is forced by European Centre for Medium Range Weather Forecasts (ECMWF) reanalyses ~~(Uppala et al., 2005; Dee et al., 2011)~~(ERA40 until 2002, ECMWF operation HIRLAM fields with an original 10-km resolution were downscaled to the 1-km model grid resolution using parameter-specific downscaling techniques (Van Pelt et al., 2016a). All meteorological variables were first linearly interpolated onto the 1-km grid, before additionally applying elevation corrections for temperature (time-dependent lapse rate), precipitation (fixed linear fractional increase with elevation), and air pressure (time-dependent exponential decay with elevation). Elevation functions for

Table 1. Overview of in situ observational data used in this study. The number of stake locations per glacier are indicated in brackets in the second column. Location abbreviations are shown and described in Fig. 1. Variable names are introduced in the text. Other abbreviations: s = summer, w = winter, C = calibration, V = validation, NPI = Norwegian Polar Institute.

Description	Location	Variables	Period	Frequency	Purpose	Source
Stake measurements	BRG (7x)	b_s, b_w	1967–2015	s,w	C	NPI
	MLB (4x)	b_s, b_w	1968–2015	s,w	C	NPI
	KNG (9x)	b_s, b_w	1987–2015	s,w	C, V	NPI
	HBR (11x)	b_s, b_w	1989–2012	s,w	C, V	Polish Acad. of Sciences
	HDF (10x)	b_s, b_w	2003–2015	s,w	C	NPI
	LNB (3x)	b_s, b_w	2004–2010	s,w	C	NPI
	AUS (27x)	b_s, b_w	2004–2013	s,w	C	Univ. of Oslo, NPI
	NBR (11x)	b_s, b_w	2006–2015	s,w	C	Uppsala & Utrecht Univ.
Weather stations	LYB	T_{air}	1975–2016	daily	V	Norwegian Meteorol. Inst.
	NA	T_{air}	1969–2015	daily	V	Norwegian Meteorol. Inst.
	AUS	T_{air}	2004–2016	daily	V	Univ. of Oslo
	KNG	SW_{net}, T_{air}	2007–2012	daily	C, V	NPI
	HDF	SW_{net}, T_{air}	2009–2012	daily	C, V	NPI
	NBR	SW_{net}, T_{air}	2009–2015	daily	C, V	Uppsala & Utrecht Univ.
Shallow cores	KNG	ρ_{sub}	1996, 2001, 2002, 2007	-	V	NPI
	AUS	ρ_{sub}	1999, 2008, 2011, 2012	-	V	Univ. of Oslo, NPI
	HDF	ρ_{sub}	2005, 2008, 2014, 2015	-	V	NPI
	NBR	ρ_{sub}	2012, 2013, 2014, 2015	-	V	Uppsala & Utrecht Univ.

temperature and air pressure were constructed per 3h time-step through respectively linear and exponential regression of the regional climate model values and their corresponding elevations; this procedure was repeated for blocks of 4×4 grid cells and regression coefficients were averaged for the whole grid to obtain a single lapse-rate for temperature and exponential decay coefficient for air pressure per time-step. Average temperature and precipitation, as well as corresponding long-term linear trends are shown in Fig. 2. Throughout the manuscript temporal trends were calculated by means of linear regression of annual time-series; non-significant trends at a 95% confidence interval were set to zero and appear as grey in the associated figures. Throughout the manuscript, significant means that a zero slope is not included in the 2σ-confidence bounds of a trend. The long-term mean temperature distribution (Fig. 2a) reveals highest temperatures at low elevation sites in the southwest, and lowest temperatures at high elevations on the Lomonosovfonna ice cap in central Svalbard. Temperature trends are significantly positive for the whole of Svalbard, with the most pronounced trends in the northeast (Fig. 2b). The long-term mean precipita-

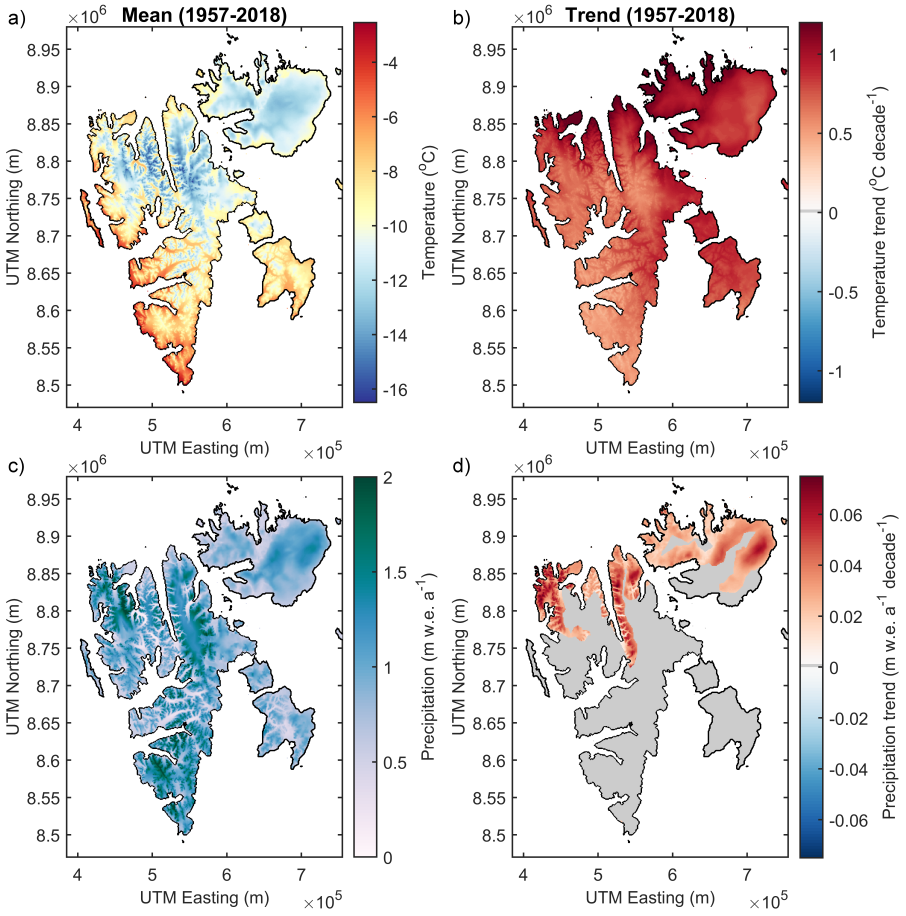

Figure 2. Long-term mean air temperature distribution (a) and trends (b). Long-term mean precipitation distribution (c) and trends (d). Non-significant trends at a 95% confidence interval are set to zero (grey).

tion distribution shows a clear elevation dependence (Fig. 2c), while long-term trends are generally found to be non-significant, except in the north, where there is a significant positive trend (Fig. 2d).

2.2 Calibration data

For model calibration, we use records of summer and winter balance (b_s, b_w) from stake measurements and net shortwave radiation (SW_{net}) observed at three automatic weather stations (Table 1).

Stake heights for a set of glaciers around Svalbard ~~(Table 1)~~ are recorded once or twice per year and, in combination with snow density and snow depth data, are converted into summer balance and winter balance estimates. Here, we use data from 82 stake locations in Svalbard, covering eight different glaciers and ice caps (Fig. 1). The Norwegian Polar Institute has collected stake data on a set of glaciers in western Svalbard, including Austre Brøggerbreen (ABB), Midtre Lovénbreen

(MLB), Kongsvegen (KNG), Holtedahlfonna (HDF) and Linnébreen (LNB); the oldest record (ABB) dates back to 1967 (e.g., Hagen et al., 1999; Kohler et al., 2007). Stake data on Hansbreen (HBR) have been collected by the Institute of Geophysics, Polish Academy of Sciences since 1989 (Grabiec et al., 2012). The University of Oslo and Norwegian Polar Institute have done made stake measurements on Austfonna since 2004 (e.g., Moholdt et al., 2010; Aas et al., 2016). Stake measurements on Nordenskiöldbreen were initiated in 2006 by Uppsala and Utrecht University (e.g., Van Pelt et al., 2012, 2018). Derived net glacier-wide mass balances of ABB, KNG, HDF and HBR are included in the World Glacier Monitoring Service database (WGMS; https://wgms.ch/).

For ABB, MLB and LNB, the dense observation network caused several stake sites to fall within one 1×1-km model grid cell, in which case we only selected the stake location closest to model grid nodes for further comparison with the model results. As a result, we include only four (out of ten) stakes on MLB, seven (out of eleven) on BRG, and three (out of eight) stakes on LNB. The winter balance data for the same set of glaciers were previously described and used in Van Pelt et al. (2016a). Summer balance is estimated using information of spring (April) and end-of-summer (September) surface height, while spring snow depth is used to distinguish between snow and ice melt. In absence of direct end-of-summer surface height measurements, the depth of the summer surface was inferred from subsequent spring stake height and snow depth data. In the accumulation zone refreezing above the summer surface is accounted for by setting an assumed end-of-summer remaining snow density of 550 kg m^{-3} (Van Pelt et al., 2018). For calculating summer and winter balance from the model output, we use fixed dates of April 15 and September 1, corresponding to average dates for spring stake data collection and end-of-summer minimum surface height, respectively.

In situ data of SW_{net} (Table 1), i.e. incoming minus reflected solar radiation, are extracted from radiation measurements at automatic weather stations in central Svalbard (NBR; Van Pelt et al., 2012), and western Svalbard (KNG and HDF; Karner et al., 2013; Van Pelt and Kohler, 2015; Pramanik et al., 2018).

2.3 Validation data

In addition to the above-described in situ data used for model calibration, we further use observed density profiles from shallow cores and air temperature time-series observed at (automatic) weather stations for validation of model results.

Shallow cores were drilled during multiple years at four locations in the accumulation zones on KNG (722 m a.s.l.), HDF (1122 m a.s.l.), NBR (1187 m a.s.l.) and AUS (758 m a.s.l.) to obtain density profiles with maximum depths ranging from 7 to 15 m below the surface (Fig. 1; Table 1). For each of the four sites we selected four firn density profiles, collected during different years on NBR (2012, 2013, 2014 and 2015), KNG (1996, 2001, 2002 and 2007), HDF (2005, 2008, 2014 and 2015) and AUS (1999, 2008, 2011 and 2012). Bulk densities are calculated over the full depth of observations and compared to simulated values over the same depth intervals.

We use a combination of air temperature records from the automatic weather stations on the glaciers AUS (Schuler et al., 2014), NBR (Van Pelt et al., 2012), and KNG and HDF (e.g., Karner et al., 2013), as well as from two land-based meteorological stations in Longyearbyen and Ny-Ålesund (data provided by the Norwegian Meteorological Institute through the eKlima data portal) for comparison with downscaled temperatures (Fig. 1; Table 1).

3 Model & Setup

3.1 Coupled modelling

A coupled modelling system is used to simulate surface and near-surface mass and energy exchange (Van Pelt et al., 2012), which has been used previously to simulate glacier mass balance, (seasonal) snow development and/or runoff in western Svalbard (e.g., Van Pelt and Kohler, 2015; Vallot et al., 2017; How et al., 2017; Winsvold et al., 2018; Pramanik et al., 2018; Deschamps-Berger et al., 2019), central Svalbard (e.g., Van Pelt et al., 2012, 2014; Vega et al., 2016; Marchenko et al., 2017b; Van Pelt et al., 2018) and on an idealized Svalbard glacier (Van Pelt et al., 2016b). In this study, the model is applied for the first time to the whole of Svalbard. At the surface, an energy balance model determines radiative (short- and longwave) and turbulent (latent and sensible) heat fluxes, and accounts for conductive heat exchange with the underlying medium, in order to calculate surface temperature and melt. Solving the surface energy balance requires input of near-surface meteorological conditions, including air temperature, cloudiness, relative humidity, air pressure and precipitation (Van Pelt et al., 2012). No wind information is needed since sensible and latent heat exchange depend solely on near-surface temperature and specific humidity gradients, following katabatic turbulent exchange relations by (Oerlemans and Grisogono, 2002). A multilayer subsurface model simulates temperature, density and water content, while accounting for snow compaction, water transport, refreezing, heat conduction, irreducible water storage, and runoff. To model seasonal snow in glacier-free terrain, the subsurface model has been extended with a soil routine (Westermann et al., 2011) to simulate permafrost thawing and freezing, and heat exchange within the soil and between the soil and overlying snow pack (if present), as described in Pramanik et al. (2018). Potential local impacts of (sparse) vegetation or surface roughness on the surface energy balance in land areas are neglected.

New in the model code used in this study, with respect to the most recent model application in Pramanik et al. (2018), is the incorporation of a new percolation scheme (Marchenko et al., 2017b), as well as the implementation of an updated albedo scheme. A deep water percolation scheme, inspired by subsurface temperature measurements on the Lomonosovfonna ice cap (Marchenko et al., 2017b), has recently been implemented to mimick the effects of preferential flow pathways in snow/firn. Additionally, we have extended the original snow age and snow depth dependent albedo scheme (Oerlemans and Knap, 1998). The original fixed characteristic time-scale for exponential decay of snow albedo due to ageing has been replaced with a temperature dependent time-scale (t^*). As in Bougamont et al. (2005), snow albedo decays fastest when the surface is melting (t^*=15 d), and for dry snow t^* linearly increases from 30 to 100 days between 0 and -10 °C. The updated albedo scheme avoids overestimation of the albedo of melting surfaces in the early melt season. Other albedo parameters, including the albedo of ice (0.39), albedo of firn (0.52), and the characteristic snow depth for albedo decay of thin snow covers (7 mm w.e.) were taken as in Van Pelt and Kohler (2015). To avoid potential systematic biases resulting from the new albedo scheme, we have included the fresh snow albedo (α_{fs}) and minimum snowfall threshold used to reset the snow albedo to the fresh snow albedo (P_{th}) in the calibration process, as described in Sect. 3.2.

The climatic mass balance refers to the sum of the surface mass balance and internal mass balance (Cogley et al., 2011) and thereby accounts for internal accumulation, i.e. refreezing and liquid water storage below the previous summer surface. Here it is calculated as the sum of mass fluxes at the surface, including precipitation (+) and moisture exchange (+/-), and mass loss

through runoff (-) at the the snow/firn to ice transition (i.e. at the surface in absence of snow). No horizontal exchange of liquid water is accounted for, i.e. runoff is assumed to occur locally.

The simulation covers the period from 1 September 1957 to 31 August 2018 with a 3-hourly temporal resolution on a distributed 1-km resolution grid. We initialize the simulation by performing a 25-year spin-up using input data for the period $1957-1982$, to generate initialized subsurface conditions. The subsurface model uses a Lagrangian grid to avoid numerical diffusion; surface mass fluxes due to precipitation, melt and moisture exchange induce thickness changes in the uppermost model layer with a thickness between 0 and 0.1 m. For both glacier-covered and land grid cells, a vertical grid consisting of 50 vertical layers is used. On glaciers, layer thickness doubles at the 15th, 25th and 35th layer through layer merging/splitting to yield vertical layer thicknesses from <0.1 to 0.8 m down to a depth of up to 20 m below the surface. In land areas, a fixed (initial) layer thickness of 0.1 m is used, extending to a depth of up to 5 m below the surface. Snow layer thickness gradually decreases over time due to snow compaction, which results in a lower total depth for grid cells with deep snow/firn columns. A central differencing scheme is used to simulate heat conduction, in which adaptive time-stepping assures stability; a zero heat flux is assumed at the lower boundary (Van Pelt and Kohler, 2015).

3.2 Calibration

Extensive calibration of energy balance model parameters in applications on Svalbard has previously been described in Van Pelt et al. (2012) and Van Pelt and Kohler (2015). Here, we use the parameter setup as described in Van Pelt and Kohler (2015), and only recalibrate constants to which melt rates have previously been found to be most sensitive, including the background turbulent exchange coefficient (C_b), the snow-to-rain transition temperature (T_{sr}), the fresh snow albedo (α_{fs}), and the snowfall threshold at which the albedo is reset to the fresh snow albedo (P_{th}). Additionally, since the simulated climatic mass balance is highly sensitive to the downscaling of precipitation from the regional climate model grid onto the 1×1 km model grid, we also calibrate the precipitation downscaling function.

In the first calibration step, multi-year records of SW_{net} observations from KNG, HDF and NBR (Table 1) were used to collectively calibrate α_{fs} and P_{th}. Since we aim to calibrate only fresh snow albedo and minimum snowfall to reset to the fresh snow albedo, we have selected SW_{net} measurements for the period April to June, when melt effects on albedo are limited, but solar insolation is high. A two-parameter exploration revealed a lowest average root-mean-square error (RMSE) between modelled and observed daily SW_{net} of 14.9 W m^{-2} for the three glaciers when choosing $\alpha_{\text{fs}} = 0.83$ and $P_{\text{th}} = 0.1$ mm w.e. hr^{-1}. RMSE values ranged from minimum 14.1 W m^{-2} on NBR to maximum 15.6 W m^{-2} on HDF, suggesting consistent performance on the three glaciers.

In the second calibration step, stake winter balance data from eight glaciers in Svalbard (Fig. 1; Table 1) were used to calibrate coefficients in the function used to project precipitation from the coarser regional climate model grid onto the finer model grid. The function describes the distribution of precipitation accounting for local topography not captured by the regional climate model, and is formulated as an elevation-dependent relation following Van Pelt et al. (2016a):

$$Pr = Pr_0\,[K_1 + (z - z_0)K_2] \tag{1}$$

Table 2. Comparison of simulated and observed b_w, b_s and b_n after calibration.

	Bias (m w.e.)			RMSE (m w.e.)		
	b_w	b_s	b_n	b_w	b_s	b_n
BRG	+0.01	+0.08	+0.08	0.14	0.35	0.39
MLB	−0.04	+0.06	+0.02	0.12	0.34	0.36
KNG	−0.12	−0.10	−0.21	0.20	0.30	0.37
HBR	−0.15	−0.01	−0.16	0.31	0.41	0.54
HDF	+0.07	+0.07	+0.14	0.14	0.26	0.30
LNB	−0.11	+0.31	+0.21	0.22	0.50	0.54
AUS	+0.20	+0.02	+0.23	0.30	0.29	0.43
NBR	+0.28	+0.14	+0.41	0.33	0.40	0.65
All data	**−0.00**	**+0.03**	**+0.02**	**0.23**	**0.34**	**0.43**

where Pr is corrected precipitation, z is elevation, Pr_0 and z_0 are spatially interpolated precipitation and elevation from the regional climate model grid onto the 1-km grid, and K_1 and K_2 are calibration coefficients. While K_1 is used to correct for potential biases in the regional climate model precipitation, K_2 represents the local precipitation-elevation gradient, which, since it is a fractional (or relative) coefficient, generates steeper absolute precipitation-elevation gradients in regions with higher overall precipitation amounts. Values from the 1-km DEM (z) will contain more detail than the z_0 values interpolated from the coarser regional climate model grid; any positive deviation of the surface height ($z - z_0 > 0$) will lead to a positive correction of the local precipitation, while a negative height deviation ($z - z_0 < 0$) will lead to a negative precipitation correction. With this approach, we account for the effect of local topography on precipitation, thereby capturing the impact of orographic lifting at scales smaller than the resolution of the regional climate model. In addition to compensation for biases in modelled precipitation (by calibrating K_1), potential surface height discrepancies at spatial scales of 10-km and greater that may arise from the use of a different DEM in the regional climate model are also automatically compensated for. Using a total of 1438 stake winter balance measurements between 1967−2015, we performed a two-parameter search to find optimum values for K_1 (1.11) and K_2 (0.0022 m^{-1}) for which a minimum RMSE of 0.23 m w.e. was found between modelled and observed winter balance (Fig. 3, Table 2). These values imply that we apply an 11% bias correction to the regional climate model precipitation and a local precipitation lapse rate of 22% per 100 m to correct for the orographic effect due to local topography. Precipitation is set to not increase further above 900 m a.s.l., in line with an observed negligible elevation gradient of b_w above this elevation on Lomonosovfonna, central Svalbard (Van Pelt et al., 2014) and Holtedahlfonna, western Svalbard (Van Pelt and Kohler, 2015). Elevations on the 1×1-km grid do not exceed 900 m a.s.l. in southern and northeastern Svalbard.

The final calibration step uses the stake summer balance data to optimize two parameters (C_b and T_{sr}) that have a strong impact on summer melt and the summer balance, while the impact on winter balance is small. A two-parameter exploration

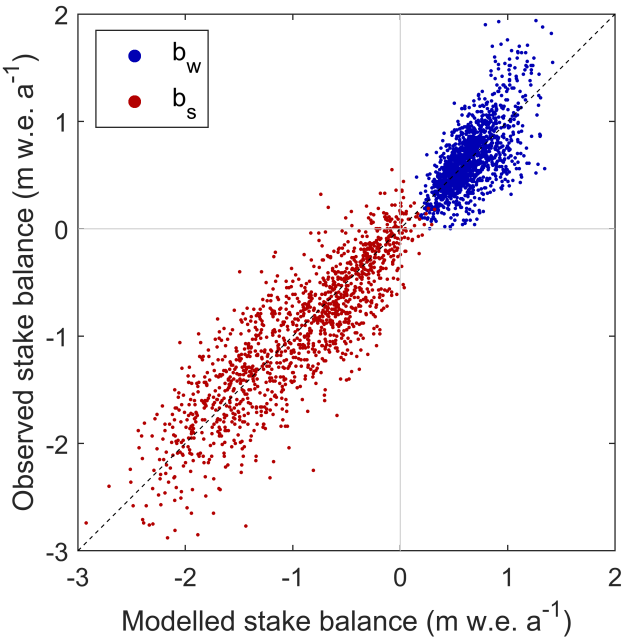

Figure 3. Simulated vs. observed summer and winter balance for all available stake data from eight glaciers (Table 1).

revealed a minimum RMSE of 0.34 m w.e. between modelled and observed summer balance for a total of 1341 observations between 1967−2015 (Fig. 3) when choosing values for $C_b = 0.0025$ and $T_{\mathrm{sr}} = 0.6$ °C.

Altogether, comparing modelled and observed net mass balance reveals an RMSE of 0.43 m w.e for all data (Table 2). For comparison, Østby et al. (2017) previously reported an RMSE of 0.59 m w.e. using a similar set of stake data for calibration. Contributing errors to the net mass balance RMSE include uncertainty in stake readings and bulk density estimation, model physics, climate forcing, and uncertainty in comparing observed point-values with simulated spatially-averaged values − the latter is particularly significant for locations where wind has a major impact on the snow distribution (e.g., Van Pelt et al., 2014). After calibration, remaining biases (modelled minus observed; calculated as the mean absolute difference) of the winter, summer and net balance are −0.00, 0.03 and 0.02 m w.e. respectively for all data, which implies low systematic errors for long-term area-averaged climatic mass balance. Comparing net mass balance for individual glaciers reveals biases ranging from −0.21 m w.e. (KNG) to +0.41 m w.e. (NBR), while RMSE is found to range from 0.30 m w.e. on HDF to 0.65 m w.e. on NBR (Table 2). Overall, we find largest errors for NBR in central Svalbard, which is primarily caused by a substantial overestimation of b_w, which in turn also induces an overestimation of b_s (underestimation of summer melt) due to a snow - albedo feedback. It is known that snow accumulation on NBR is highly influenced by wind driven snow redistribution and erosion (Van Pelt et al., 2014). This may explain the overestimation of snow accumulation in our modelling of NBR, since effects of wind on snow accumulation are not accounted for in the downscaling of regional climate model precipitation. On the other hand, underestimation of b_w is apparent for KNG and HBR (Fig. 3, Table 2), which results from underestimated orographic precipitation at high elevations on these glaciers. ~~In general, the strong connection between uncertainty in~~ Nevertheless, high-elevation biases

of b_w ~~and b_n emphasises the need for precipitation calibration for accurate CMB modelling~~do not arise on the two glaciers extending above 1000 m a.s.l., which indicates that the b_w offsets on KNG and HBR are not a systematic feature for high elevation sites in general. The relative lack of stake observations at heights above 1000 m a.s.l. implies increased uncertainty of modelled precipitation estimates at these elevations (Möller et al., 2016).

3.3 Validation

To assess how well the model is able to simulate time-evolution of glacier-wide CMB, we compare simulated glacier-average winter CMB (B_w), summer CMB (B_s) and net CMB (B_n) for HBR and KNG against observation-based estimates from the WGMS database (Fig. 4). The long-term WGMS records in Svalbard from BRG and MLB are excluded due to a lack of model grid cells falling within the glacier outlines (9 for BRG and 5 for MLB); model grids of HBR and KNG include 66 and 110 grid cells respectively. Simulated annual net CMB values show good agreement with the WGMS values for both KNG ($R = 0.86$; $P < 0.001$; RMSE$= 0.18$ m w.e. a^{-1}) and HBR ($R = 0.67$; $P < 0.001$; RMSE$= 0.27$ m w.e. a^{-1}). Furthermore, long-term simulated and observed net CMB trends are consistent for both KNG (modelled -0.18 ± 0.11 m w.e. a^{-1} decade^{-1}; observed -0.10 ± 0.13 m w.e. a^{-1} decade^{-1}) and HBR (modelled 0.02 ± 0.20 m w.e. a^{-1} decade^{-1}; observed -0.05 ± 0.19 m w.e. a^{-1} decade^{-1}).

Air temperature and precipitation are the main meteorological drivers of spatial patterns and trends in CMB and its components. As discussed in Sect. 3.1, the downscaling of precipitation has been optimized using in situ winter balance data from multiple sites in Svalbard. Here, we validate the temperature forcing by comparing downscaled daily 2-m temperature with in situ temperature records (recorded at $1-4$ m heights) from ~~five~~ six sites in Svalbard (Table 1; Sect. 2.3). Results are summarized in Table 3. We find very high correlations ($R = 0.95-0.97$; $P < 0.001$), RMSE ranging between 2.0 °C (KNG) and 4.6 °C (HDF), and biases ranging from -2.3 °C (AUS) to $+0.7$ °C (KNG). In general, we find good agreement between downscaled and observed temperatures for both glacier and non-glacier terrain in different regions in Svalbard. The largest bias and RMSE are found at AUS in northeast Svalbard, which can be ascribed to a substantial underestimation of air temperature during the cold season (September$-$May) of -3.2 °C, whereas the summer (June$-$August) air temperature bias is small (+0.4 °C).

Finally, in situ observations from shallow cores (Sect. 2.3) are used to validate bulk density (ρ_{sub}) simulated at AUS, HDF, NBR and KNG during four years down to depths of $7-15$ m (Table 1). For three sites, we find negative model biases for ρ_{sub} of -25 kg m^{-3} (NBR), -30 kg m^{-3} (AUS) and -38 kg m^{-3} (HDF). On KNG, a positive bias of $+48$ kg m^{-3} is found. Table 2 shows that KNG is the only site of the four experiencing a negative b_w bias. Based on this, we argue that an underestimation of accumulation explains the overestimation of ρ_{sub} at KNG, and vice versa at NBR, AUS and HDF. An inverse relation between ρ_{sub} and accumulation follows from 1) the parametrization used for gravitational settling (Ligtenberg et al., 2011), and 2) an increased significance of refreezing on the vertical density distribution where accumulation rates are low (subsurface layers remain closer to the surface for a longer time and will hence experience refreezing of stored water in the cold season during more years).

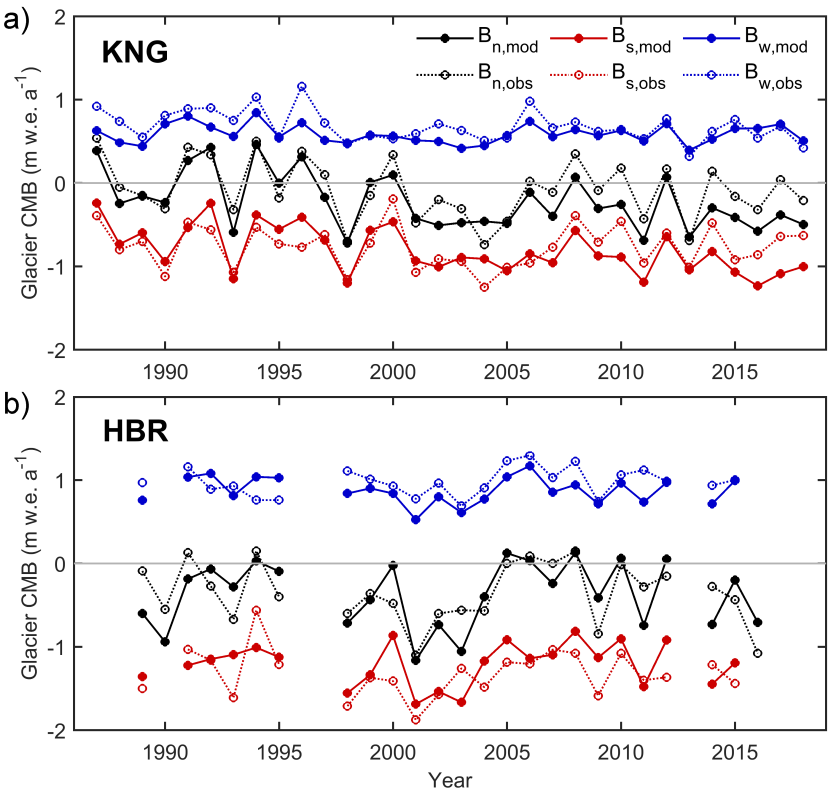

Figure 4. Comparison of simulated glacier-wide summer, winter and net mass balance against WGMS records for KNG (a) and HBR (b).

Table 3. Comparison of downscaled and observed air temperatures at glacier- and land-based weather stations.

Location	Elevation (m a.s.l.)	Surface type	# of observ. (days)	R	bias (°C)	RMSE (°C)
LYB	28	land	14963	0.97	+0.4	2.6
NA	8	land	17066	0.96	−0.1	2.3
KNG	520	glacier	1374	0.97	+0.7	2.0
HDF	680	glacier	1334	0.95	+0.1	3.1
NBR	519	glacier	1554	0.95	−0.8	2.9
AUS	350	glacier	4386	0.92	−2.3	4.6

4 Results & Discussion

In this section, we present and discuss spatial patterns and trends of simulated CMB, ELA, subsurface conditions, refreezing and runoff over the period 1957−2018.

4.1 Climatic mass balance & ELA

Averaged over the entire simulation period, we find a spatial mean glacier ~~CMB~~ net CMB (hereafter just CMB) of +0.09 m w.e. a^{-1}, which is comparable to Østby et al. (2017) [+0.08 m w.e. a^{-1} over the period 1957−2014] and more positive than a recent estimate by Möller and Kohler (2018) [−0.03 m w.e. a^{-1} over the period 1957−2010]. The spatial CMB distribution in Fig. 5a reveals most negative CMB values (down to −2.5 m w.e. a^{-1}) at low elevations in southern and western Svalbard, and most positive CMB (up to 1.3 m w.e. a^{-1}) at high-elevation sites on the Lomonosovfonna ice cap (central Svalbard). Assuming a frontal ablation rate equivalent to −0.18 m w.e. a^{-1} (Blaszczyk et al., 2009), and negligible basal melting, we estimate a total mass balance of −0.09 m w.e. a^{-1}. In the latter calculation it is implicitly assumed that frontal ablation rates from Blaszczyk et al. (2009) for the early 2000s apply during the whole simulation period. We find significantly negative CMB trends in southern and central Svalbard, while trends are not significant in the north (Fig. 5b). On average, a significantly negative CMB trend of −0.06±0.04 m w.e. a^{-1} $decade^{-1}$ is found (Fig. 5c). For comparison, a more negative trend of −0.14 m w.e. a^{-1} $decade^{-1}$ was reported by Østby et al. (2017) over the period 1957−2014, although it was argued that the trend may have been overestimated based on a comparison of long-term CMB at a single stake site on MLB. Conversely, Lang et al. (2015) found a weaker negative CMB trend (−0.03 m w.e. a^{-1} $decade^{-1}$) for 1979−2013, which is however not significantly different from our trend of −0.07±0.08 m w.e. $decade^{-1}$ over the same period. Significant trends of opposite sign are found for the winter balance (+0.02±0.01 m w.e. a^{-1} $decade^{-1}$) and summer balance (−0.08±0.03 m w.e. a^{-1} $decade^{-1}$), suggesting that a winter accumulation increase compensates for some of the increased summer ablation. Inter-annual variability of net CMB correlates strongly with both summer (June−August) air temperature ($R = 0.78$; $P < 0.001$) and annual (September−August) precipitation ($R = 0.60$; $P < 0.001$), while no significant correlation exists between annual temperature and net CMB ($R = 0.10$; $P > 0.1$).

The average ELA of the entire glacierized area in Svalbard is 367 m a.s.l. for 1957−2018. The ELA distribution resembles an earlier observation-based map by Hagen et al. (2003) with highest ELA (>700 m a.s.l.) in relatively dry regions in northern Spitsbergen and lowest ELA (<200 m a.s.l.) induced by cold conditions in northeastern Svalbard (Fig. 6a). Significant positive ELA trends are apparent for all of Svalbard, except for the most northern parts (Fig. 6b), where increased precipitation (Fig. 2d) offsets an ELA increase due to a melt increase. Based on annual ELA time-series, we find a significant mean positive ELA trend of 17±12 m a.s.l. $decade^{-1}$, which is slightly less than a previously reported trend of 25 m a.s.l. $decade^{-1}$ over 1961−2012 in Van Pelt et al. (2016a). As a result of upward ELA migration, the accumulation area ratio (AAR) has decreased at an absolute rate of −4% per $decade^{-1}$; the average AAR for 1957−2018 equals 65% with annual values ranging from 17% (1997−1998) to 91% (1964−1965). As previously discussed in Van Pelt and Kohler (2015), surface melt is amplified due to substantial lowering of the albedo in the new ablation areas exposed by the retreating ELA. The average albedo over the

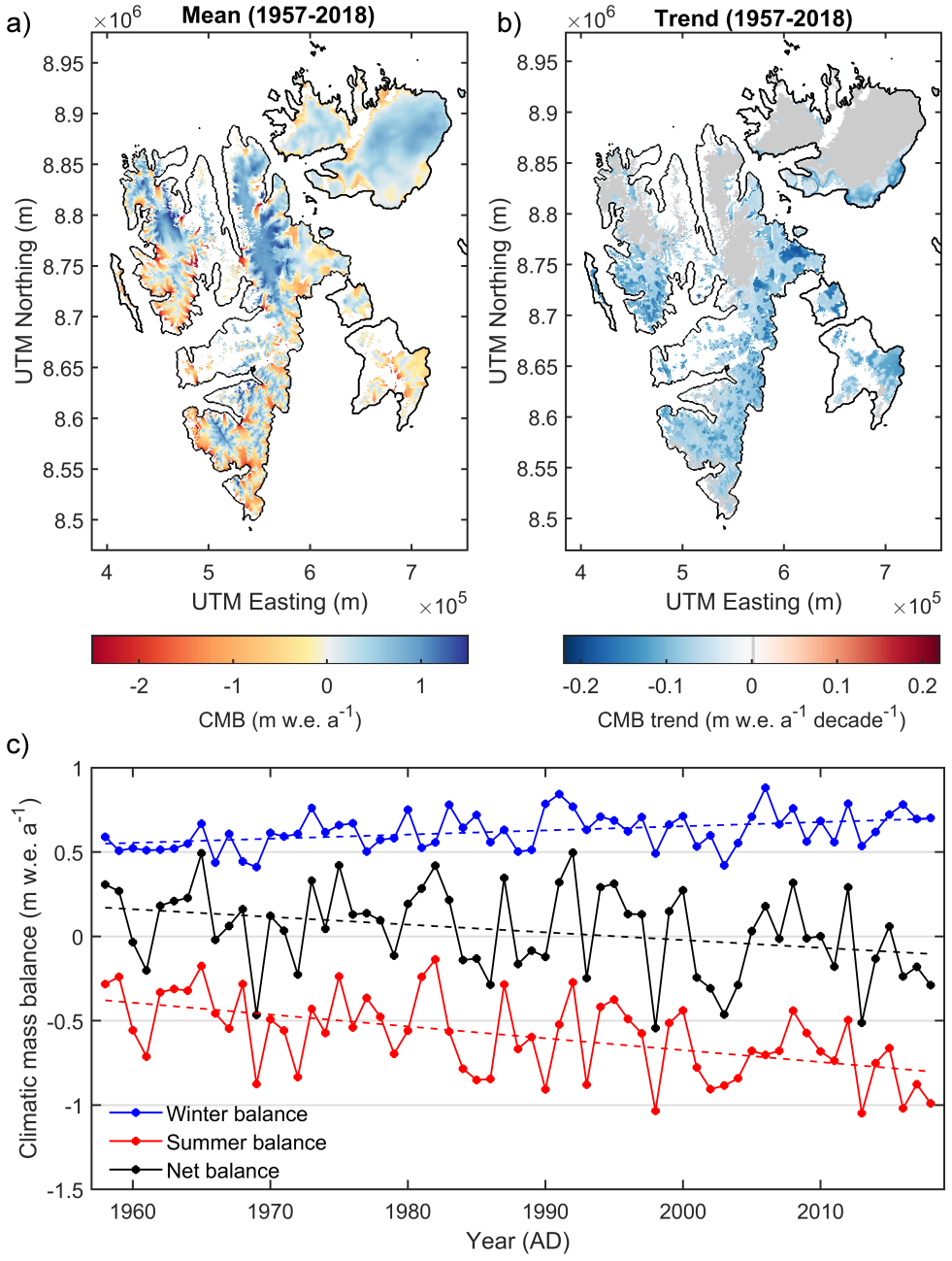

Figure 5. Long-term mean spatial CMB distribution (a) and trends (b). In (c) time-series of area-averaged annual mean summer, winter and net CMB (solid lines) and linear trends (dashed lines) are shown. In (c) years are defined based on a mass balance year between 1 September (preceding year) and 31 August.

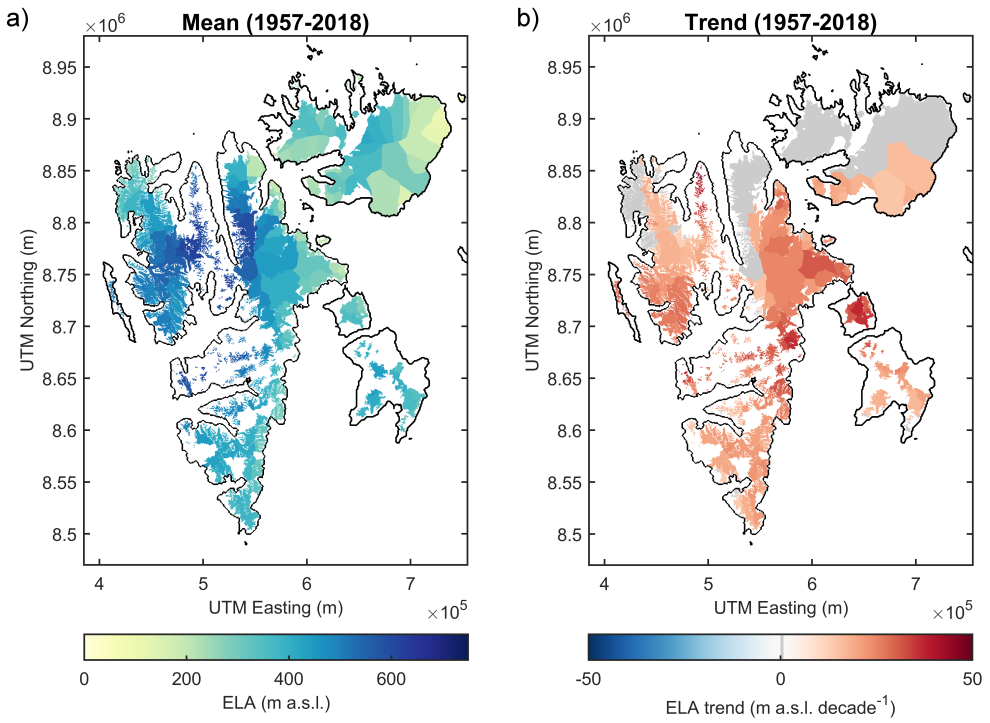

Figure 6. Long-term mean spatial ELA distribution (a) and trends (b). Data are averaged per glacier basin, based on the glacier outline database in König et al. (2014).

simulation period is 0.76 for all glaciers in Svalbard, with a significant negative trend of -0.004 ± 0.001 decade^{-1} (locally down to -0.024 decade^{-1}), inducing an average 2% decade^{-1} increase of absorbed solar radiation.

4.2 Glacier subsurface conditions

As a collective measure of density and depth of snow and firn in glacierized areas, we quantify the total pore space down to a depth of 14 m below the surface (P_{14}), expressed in m^3 m^{-2}, and shown in Fig. 7a-b. Large accumulation zones with P_{14} exceeding 5 m^3 m^{-2} are found at high elevations on the three major ice caps in northern Svalbard (Holtedahlfonna, Lomonosovfonna and Austfonna); smaller accumulation zones with generally lower P_{14} prevail in southern Svalbard (Fig. 7a). Trends in P_{14} (Fig. 7b) are most negative (down to -0.6 m^3 m^{-2} decade^{-1}) in elevation bands close to the long-term mean ELA, as upward migration of the firn line causes a major decline in firn depth. As a result, the most negative P_{14} trends are found in central Svalbard, where ELA trends are most positive (Fig. 6b). For $1957-2018$, average P_{14} for the glacierized area, i.e. including both ablation and accumulation zones, equals 2.3 m^3 m^{-2}; the average trend is significantly negative (-0.09 ± 0.03 m^3 m^{-2} decade^{-1}), and equivalent to a 4% decrease of P_{14} per decade.

The distribution and trends of deep temperature (T_{14}), defined here as the temperature at 14 m below the surface, are shown in Fig. 7c-d for the glacierized area of Svalbard. The T_{14} distribution reveals a marked transition around the ELA

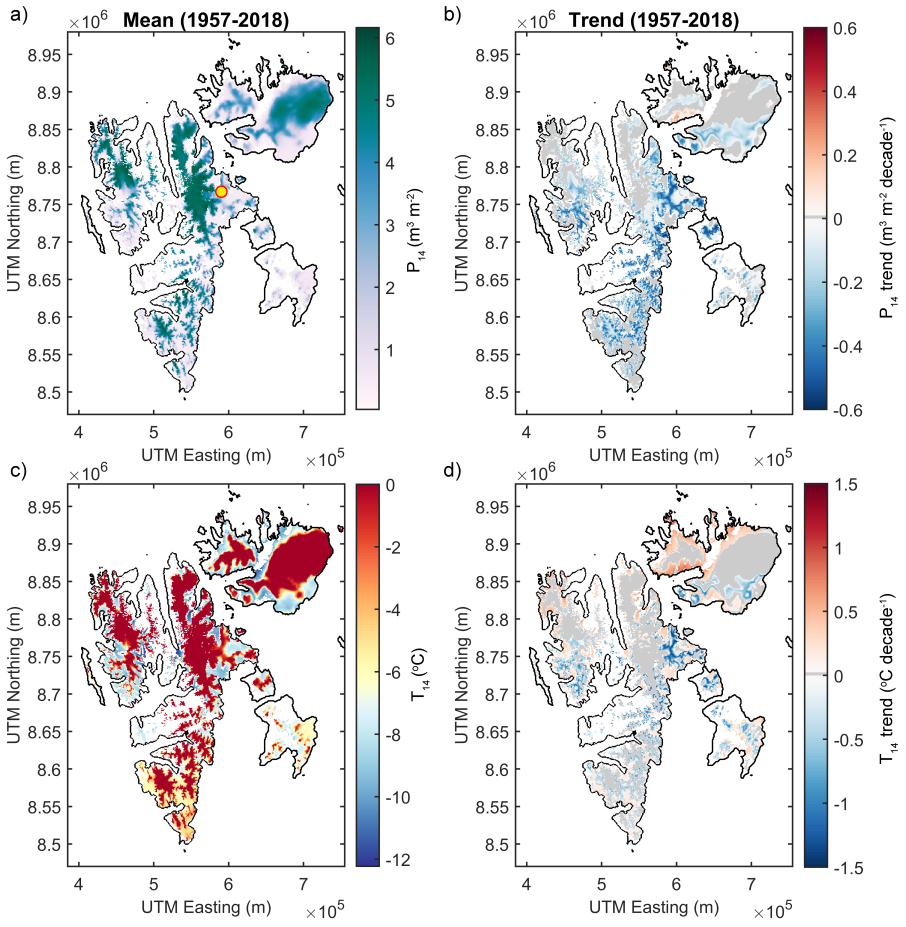

Figure 7. Long-term mean P_{14} distribution (a) and trends (b). Long-term mean T_{14} distribution (c) and trends (d). The corresponding location of the subsurface profiles in Fig. 8 is marked with a red circle in (a).

from cold (non-temperate) conditions in the ablation zones to temperate conditions in accumulation areas for all glaciers in Svalbard. This thermodynamic structure is common for Svalbard glaciers (Björnsson et al., 1996; Pettersson, 2004), and has previously been linked to the high significance of (deep) percolation and refreezing in accumulation zones (e.g., Van Pelt et al., 2012, 2016b). Temperate T_{14} conditions also precondition the potential formation of perennial firn aquifers, which have been detected using ground-penetrating radar on Holtedahlfonna in western Svalbard (Christianson et al., 2015), and recently also on Lomonosovfonna in central Svalbard (R. Pettersson, unpublished data). The widespread occurrence of temperate deep firn suggests the likelihood of perennial firn aquifers in other accumulation zones on Svalbard. On Austfonna, a radar survey in 2014 showed a strong reflector over large distances across the summit area, which potentially results from deep slush water storage (T. Dunse, unpublished data). In addition to temperature, other factors affecting firn aquifer development include surface topography (steering water flow in the aquifer), and the potential for englacial drainage through cracks, crevasses and

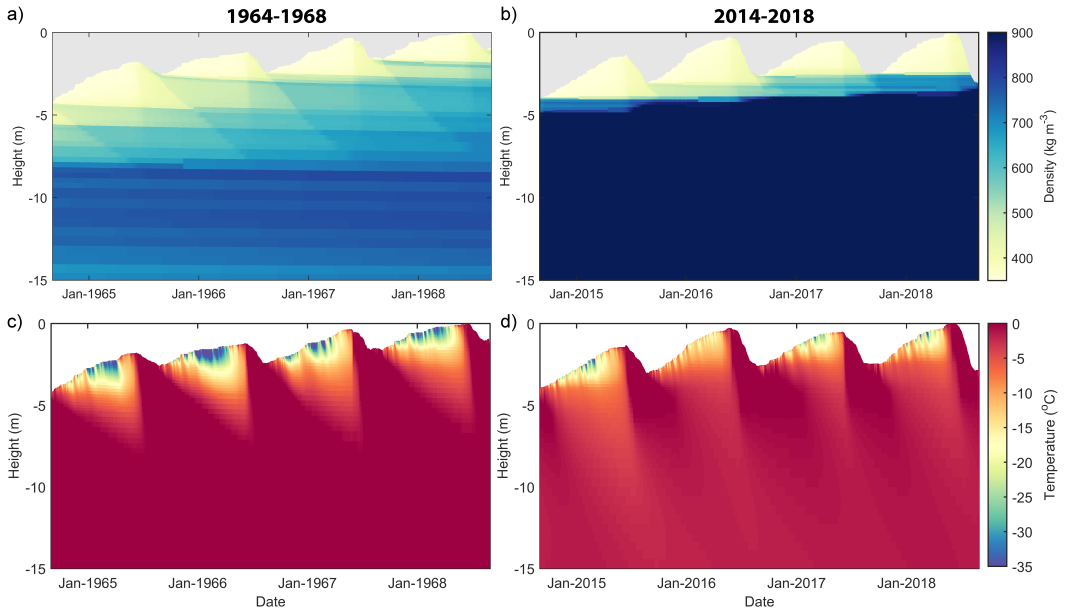

Figure 8. Subsurface density (a-b) and temperature (c-d) evolution during the periods 1964−1968 (a&c) and 2014−2018 (b&d). The corresponding geographic location of the site is indicated in Fig. 7a.

moulins. Our results suggest that even the highest (coldest) accumulation zones in Svalbard have average temperate deep firn conditions. This is in line with recent measurements (2012−2015) on Lomonosovfonna at 1200 m a.s.l. (Marchenko et al., 2017b), but does not agree with earlier findings of sub-temperate conditions at ice core drill sites on Lomonosovfonna in 1997 (Van de Wal et al., 2002) and Holtedahlfonna in 2005 (Beaudon et al., 2013). However, we infer that both these drill sites were likely drilled in locations with isolated cold deep temperature conditions within otherwise temperate accumulation zones, as confirmed by the widespread presence of perennial firn aquifers. Cold deep temperature conditions may occur locally at wind-exposed sites, e.g. on an ice divide or ridge, as accumulation rates are typically lower due to wind erosion, which has a cooling effect on deep firn (Kuipers Munneke et al., 2014). Additionally, we infer that the convex topography of ice divides promotes efficient drainage and reduces the significance of latent heat release by refreezing. For both drill sites, reported accumulation rates estimated from the ice cores of 0.41 m w.e. a^{-1} (Lomonosovfonna, 1950−1997, Pohjola et al., 2002) and 0.50 m w.e. a^{-1} (Holtedahlfonna, 1963−2005, Van der Wel et al., 2011) are indeed substantially lower than observed at the nearest stakes on Holtedahlfonna (0.98 m w.e. a^{-1} for 2003−2015) and Lomonosovfonna (0.85 m w.e. a^{-1} for 2006−2015). Long-term trends of T_{14} (Fig. 7d) reveal a warming trend in ablation zones and a cooling trend in former accumulation zones that recently became ablation zone due to upward migration of the firn line; the average trend is weakly negative (-0.03 ± 0.03 ^{o}C decade^{-1}).

An example of firn density and temperature evolution during two periods (1964−1968 and 2014−2018) at a site close to the long-term mean ELA in central Svalbard is shown in Figure 8 (location indicated in Fig. 7). During 1964−1968, deep temperature is consistently at the melting point (Fig. 8c) and no thick ice layers are present in the upper 10−15 m of firn (Fig.

8a). During 2014−2018, the same site is still in the lower accumulation zone, but now firn density is markedly increased, with impermeable ice below a depth of 1−3 m below the surface (Fig. 8b). It is noteworthy that similar firn developments have recently been observed in the lower accumulation zone in western Greenland (Cox et al., 2015; Machguth et al., 2016)~~and~~ , the Canadian Arctic (Bezeau et al., 2013) ~~,~~ and the Larsen C ice shelf, Antarctica (Hubbard et al., 2016; Bevan et al., 2017) and have been argued to potentially affect horizontal drainage. As firn densifies, percolating water more readily runs off, and the potential for deep water storage and subsequent refreezing is reduced. In response to reduced refreezing, as well as faster heat conduction, deep firn/ice temperatures in 2014−2018 are no longer temperate at this site (Fig. 8d).

4.3 Refreezing

The distribution of refreezing for both glacier-covered and land areas reveals that the highest refreezing rates (up to 0.41 m w.e. a^{-1}) are in the accumulation zones (Fig. 9a), where percolating water can be stored deep in snow/firn and refreeze over the course of the winter season (Van Pelt et al., 2016b). The lowest refreezing rates (<0.05 m w.e. a^{-1}) are at low elevations, i.e. in coastal regions and valleys, where thin seasonal snow packs develop over winter, thereby limiting the potential for refreezing. For 1957−2018, we find average refreezing rates of 0.24 m w.e. a^{-1} and 0.14 m w.e. a^{-1} for the glacier-covered and land areas respectively. For comparison, Østby et al. (2017) found comparable refreezing rates of 0.22 m w.e. a^{-1} for all glaciers in Svalbard during 1957−2014. ~~On average, we find that 25% of melt and rainwater is refrozen, implying a substantial reduction of runoff. It should however be acknowledged that indirect effects after refreezing, in particular heat release in the snow pack, will induce additional melt, which will reduce the net impact of refreezing on runoff (Van Pelt et al., 2016b).~~ Long-term ~~trends~~ refreezing trends (Fig. 9b) reveal significantly decreasing refreezing rates (down to −0.03 m w.e. $decade^{-1}$) primarily at elevations around the ELA in response to firn line retreat~~(Fig. 9b).~~ . No significant trends ~~in~~ of refreezing are found in high accumulation zones, which implies the likely growth of perennial firn aquifers during the simulation period since input from surface melt and rainfall shows a clear positive trend ($+0.058 \pm 0.022$ m w.e. $decade^{-1}$). On average, we find comparable negative trends for the glacier-covered areas (-0.007 ± 0.002 m w.e. a^{-1} $decade^{-1}$) and land areas (-0.008 ± 0.002 m w.e. a^{-1} $decade^{-1}$), implying a much faster *relative* decrease of refreezing on land (−6.0% $decade^{-1}$) than on glaciers (−2.9% $decade^{-1}$). ~~As~~

The fraction of melt and rain that refreezes, i.e. the refrozen fraction, is on average 0.27 or 27% (Fig. 9c), implying a substantial reduction of runoff. It should however be acknowledged that indirect effects after refreezing, in particular heat release in the snow pack, will induce additional melt, which will reduce the net impact of refreezing on runoff (Van Pelt et al., 2016b). The spatial distribution of the refrozen fraction (Fig. 9c) reveals minimum values in coastal land areas in the southwest, where melt and rainfall rates are high and winter cooling is limited; maximum values are found at high elevations in central Svalbard (Lomonosovfonna), where melt and rainfall are small and most percolating water is retained due to early melt season refreezing of percolating water and winter-time refreezing of stored irreducible water. The refrozen fraction trends (Fig. 9d) show a Svalbard-wide significant decrease (average -0.03 ± 0.01 $decade^{-1}$) with most pronounced negative trends in cold (high-altitude) regions in central and northern Svalbard.

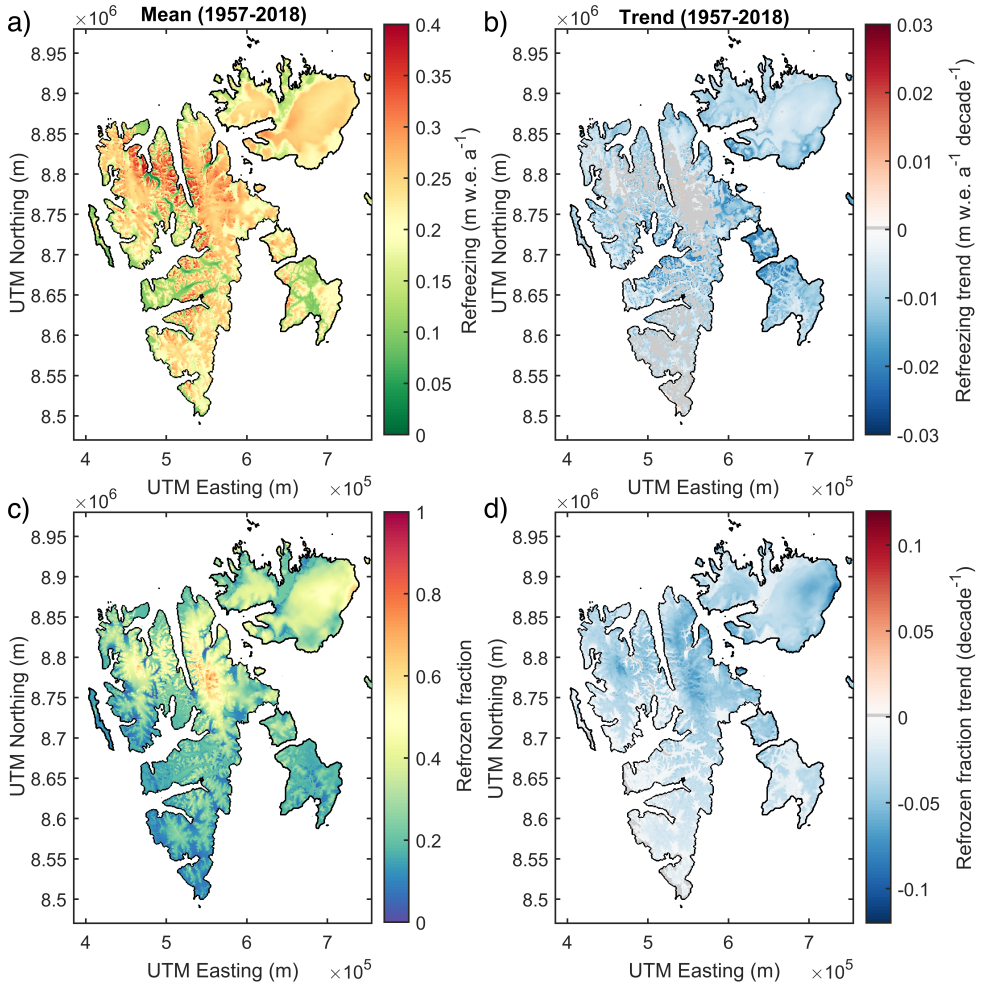

Figure 9. Long-term mean spatial refreezing distribution (a) and trends (b). Long-term mean spatial refrozen fraction distribution (c) and trends (d).

Overall, we find that no sites have a long-term mean refrozen fraction close to 1 (Fig. 9c), implying that deep cold firn has been absent throughout the simulation period~~,~~. This implies that there is no potential for additional refreezing buffering higher melt rates in a warming climate, which is similar to what has been suggested for peripheral glaciers and ice caps of the Greenland ice sheet beyond a 'tipping point' in 1997 (Noël et al., 2017). The consistently negative refreezing trend throughout the simulation period in this study suggests that the tipping point would have occurred already prior to the start of the simulation in 1957. Similar long-term negative refreezing trends were previously described by Noël et al. (2018) for ice caps in the southern Canadian Arctic. Future projections of refreezing in Svalbard show that while there will be less refreezing in the early melt season due to reduced winter cooling (reducing the cold content required for refreezing) and shrinking accumulation zones, at the same time winter-time refreezing during and after rainfall and melt events will increase (Van Pelt et al., 2016b).

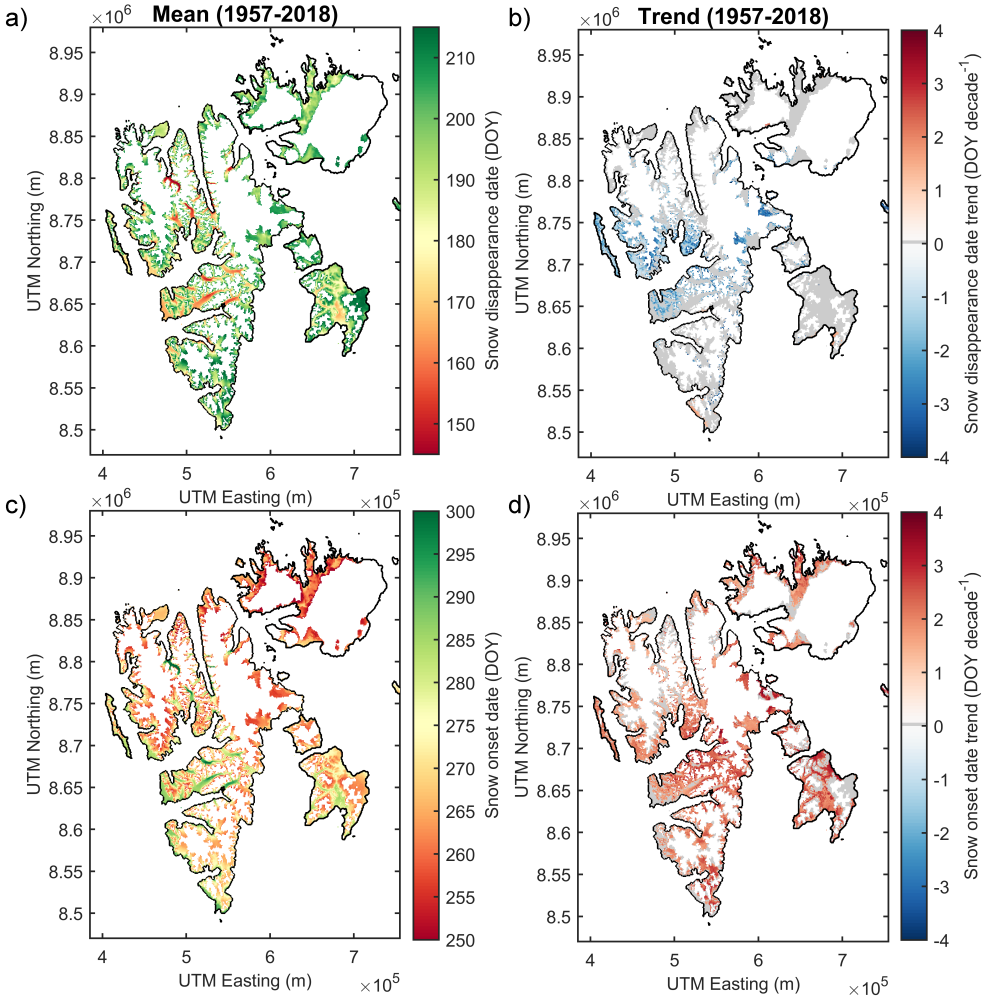

Figure 10. Long-term mean spatial snow disappearance date distribution (a) and trends (b). Long-term mean spatial mean snow onset date distribution (c) and trends (d). Snow onset and disappearance dates are only calculated for sites where snow melts completely in summer during at least half of the years in the simulation.

4.4 Seasonal snow cover duration

Land areas and glacier ablation zones in Svalbard experience snow-free conditions during the summer season. The extent of the snow-free season is defined by the snow disappearance date, which we define to occur when snow amount first drops below a threshold (1 cm w.e.), and the snow onset date, which we define as the first date on which snow (>1 cm w.e.) accumulates and remains until next year. Long-term mean distributions of the snow disappearance and onset dates (Fig. 10a and c) show that the earliest snow disappearance (late May) and latest snow arrival (late October) are to be found in the relatively dry valleys of central Svalbard. Trends in the snow disappearance date are primarily controlled by winter accumulation (cumulative

snowfall) and melting. We find negligible trends of the snow disappearance date for most of Svalbard, except for parts of central Svalbard, where snow disappears earlier over time (up to 4 days decade^{-1}, Fig. 10b). There is however no significant average snow disappearance trend for all of Svalbard (0.0 ± 0.9 days decade^{-1}), suggesting that, on average, the slight increase in precipitation, generating thicker winter snow packs, is compensated for by an earlier onset of melting. The snow onset date (September−October) is strongly influenced by air temperature affecting both precipitation type (snow/rain) and potential melt of freshly fallen snow. In response to the substantial autumn warming (Førland et al., 2011; Van Pelt et al., 2016a), snow onset trends are significantly positive (up to $+4$ days decade^{-1}) for most of Svalbard (Fig. 10d), leading to a significant mean positive snow onset date trend of $+1.4 \pm 0.9$ days decade^{-1}. ~~For comparison, Van Pelt et al. (2016a) found comparable trends~~ The above discrepancy in trends for snow disappearance and onset dates was previously also found in Van Pelt et al. (2016a), where estimates of $+1.8$ days decade^{-1} for the snow onset date and $+0.7$ days decade^{-1} for the snow disappearance date over the shorter period 1957−~~2012.~~ 2012 were presented.

4.5 Runoff

The long-term mean runoff distribution (Fig. 11a) shows local discharge is apparent across all of Svalbard, with the highest rates (> 3 m w.e. a^{-1}) in the glacier ablation zones in southern Svalbard, and the lowest rates < 0.3 m w.e. a^{-1} at the high elevations of the Lomonosovfonna ice cap in central Svalbard. Here, runoff refers to the amount of water originating from melt and rainfall at the surface and available at the base of the snow/firn pack (if present) or ice/soil surface after accounting for retention by refreezing and liquid water storage. Melt rates on land are limited to the amount of seasonal snow accumulating during the cold season, and therefore generate much lower runoff rates than nearby glacier sites at similar elevations (Fig. 11a). As a result, the area-averaged runoff from glaciers (0.81 m w.e. a^{-1}) is higher than the runoff from land (0.63 m w.e. a^{-1}), despite the lower mean elevation of the land cells compared to the glacier grid. Trends of runoff over the simulation period (Fig. 11b) are generally not significant for land, but are significantly positive for glaciers, with largest increases (up to 0.2 m w.e. a^{-1} decade^{-1}) in ablation zones recently exposed by the retreating ELA. Time-series of runoff in Gt a^{-1} (Fig. 11c) show average runoff of 10.6 and 34.3 Gt a^{-1} from land and glacier-covered areas respectively, contributing to a total average annual runoff of 44.9 Gt a^{-1}. Runoff from land is primarily controlled by precipitation, and as a result the long-term trend is not significant ($+0.2 \pm 0.3$ Gt a^{-1} decade^{-1}). Conversely, runoff from glaciers is primarily controlled by summer melt, and is found to increase markedly over the simulation period ($+3.7 \pm 1.3$ Gt a^{-1} decade^{-1}), in accordance with decreasing CMB. As a result, total runoff increases by $+3.9 \pm 1.4$ Gt a^{-1} decade^{-1}, which is equivalent to a 9% decade^{-1} increase in runoff. The contrast in trends of runoff from glaciers and land implies a substantial decrease in the relative contribution of land runoff to total runoff from ∼30% to around ∼20% between 1957 and 2018. Finally, the Svalbard averaged trend in runoff ($+0.065 \pm 0.023$ m w.e. decade^{-1}) is substantially larger than the trend in the sum of melt and rainfall ($+0.058 \pm 0.022$ m w.e. decade^{-1}), which is fully explained by a negative trend in refreezing (-0.007 ± 0.002 m w.e. decade^{-1}). That means that 11% of the increase in runoff can be explained by reduced refreezing over the simulation period.

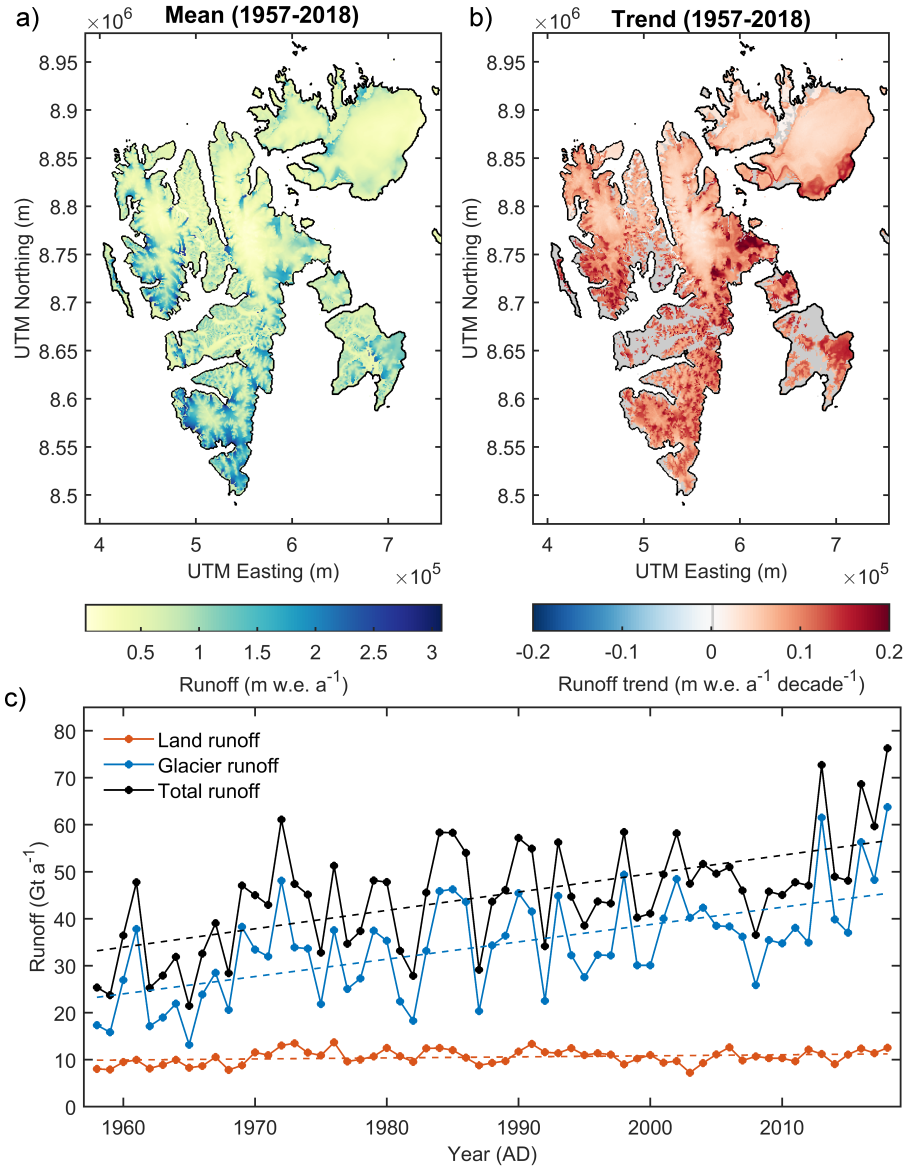

Figure 11. Long-term mean spatial runoff distribution (a) and trends (b). In (c) time-series of area-averaged annual glacier, land and total runoff (solid lines) and linear trends (dashed lines) are shown. Years in (c) are defined between 1 September (preceding year) and 31 August.

4.6 Uncertainties

As described in Sect. 3.2 and in previous studies using the same model in Svalbard (Van Pelt et al., 2012; Van Pelt and Kohler, 2015; Marchenko et al., 2017b; Pramanik et al., 2018), observational data have been extensively used for calibration, thereby

reducing errors in downscaling climate input, solving the energy balance and simulating subsurface conditions. Nevertheless, uncertainty remains, and here we briefly summarise the main remaining sources of errors.

First, we assumed the elevation grid and glacier masks to be fixed throughout the simulation period ~~.~~ (Sect. 2.1). As both elevations and masks are based on observational data collected after 1990, this may introduce ~~biases~~ CMB deviations relative to what would be observed on a time-evolving glacier surface, in particular during the first decades of the simulation. ~~The uncertainty~~ These deviations due to elevation ~~errors is~~ offsets are most pronounced near glacier fronts where thinning rates between $1-2$ m a^{-1} have been observed in the $2-4$ decades preceding $2003-2007$ (Nuth et al., 2010). With a mean balance gradient of 0.002 m w.e. a^{-1} m^{-1}, this would generate a potential underestimation of CMB of $0.1-0.2$ m w.e. a^{-1} during the first years of the simulation at sites near the glacier snout; at higher elevations errors will be markedly smaller. Typical ~~errors~~ deviations associated with the use of a fixed glacier mask, compared to a time-dependent glacier mask, have previously been quantified for Svalbard for a similar simulation period at around $0.02-0.04$ m w.e. a^{-1} (Østby et al., 2017). We assume similar ~~errors~~ values would apply here. It is noteworthy that CMB errors induced by a fixed mask will be of opposite sign as errors induced through the use of a fixed DEM (underestimation of glacier extent in the early decades leads to a too positive CMB, while underestimation of elevations induces a too negative CMB), meaning that some of the above ~~errors~~ deviations are likely to cancel each other out. Largest ~~errors~~ deviations will apply to glaciers that surged during the simulation period. ~~The~~ Note that the above deviations should not be regarded as errors, it only implies we present and analyze a different quantity (reference mass balance) than what would be observed on a transient glacier surface. Altogether, the use of a fixed mask and elevations has the advantage that all presented trends in climatic mass balance and related products can be attributed to changes in the climate forcing, and we can exclude any influences from dynamically induced geometric changes.

A second source of error comes from uncertainty in the climate input, more specifically the air temperature and precipitation forcings, to which climatic mass balance, seasonal snow development and derived products are most sensitive. Validation of air temperature against glacier- and land-based measurements (Sect. 3.3) revealed good correlation and generally low biases. In turn, winter balance data were used to optimize the downscaling of precipitation, also returning good correlation and negligible biases (Sect. 3.2). Nevertheless, on average we find a substantially higher snowfall rate (0.89 m w.e. a^{-1}) than previously reported rates of 0.61 m w.e. a^{-1} by Østby et al. (2017) for $1957-2014$, and 0.44 m w.e. a^{-1} by Lang et al. (2015) for $1979-2013$. Østby et al. (2017), however, found that winter accumulation was generally underestimated, primarily at higher elevations, based on a comparison with similar stake winter balance data as used in this study (Fig. 11 in Østby et al., 2017). Furthermore, Lang et al. (2015) only validated their precipitation estimates against meteorological station data in Svalbard, which are known to suffer severely from undercatch (Førland and Hanssen-Bauer, 2000). Nevertheless, we cannot rule out potential biases in our snowfall/precipitation estimates, in particular because all stakes used for calibration are located on glaciers and primarily along their centerlines, which may induce potential biases (e.g., Nuth et al., 2012; Deschamps-Berger et al., 2019). Additionally, the relatively coarse spatial resolution of the regional climate model forcing may cause spatial precipitation fields to miss some of the impacts of terrain on the precipitation distribution, even though this is to some extent compensated for by the precipitation downscaling, which accounts for local elevation. Finally, as also discussed in Sect. 3.2, the inconsistency between the point-wise nature of stake observations and gridded model output representing processes within

1 km^2 cells, induces uncertainty in the comparison of climatic mass balance components. This is likely to be most pronounced for the b_w comparison in wind-affected areas across Svalbard, since b_w is known to vary over distances much smaller than the 1 km horizontal resolution used here~~(e.g., Winther et al., 2003; Van Pelt et al., 2014)~~, primarily due to wind-driven snow redistribution (e.g., Winther et al., 2003; Jaedicke and Gauer, 2005; Grabiec et al., 2011; Van Pelt et al., 2014).

A third source of uncertainty are the modelling errors, which includes uncertainties related to solving the energy balance, simulating subsurface conditions as well as model initialization. Descriptions of the heat fluxes comprising the surface energy balance have been optimized against observational data in glacier basin studies on Nordenskiöldbreen (Van Pelt et al., 2012) and around Kongsfjorden (Van Pelt and Kohler, 2015), as also discussed in Sect. 3.2. ~~With the~~ Energy balance parameters were taken as in the aforementioned studies, with the exception of the ~~new albedo parametrization, which we calibrated against observed SW_{net} data , other energy balance parameters were taken as in the aforementioned studies.~~ fresh snow albedo (α_{fs}), the associated minimum snowfall threshold (P_{th}), and the background turbulent exchange coefficient (C_b), which were calibrated against observational data (Sect. 3.2). The new albedo scheme assumes that previously used values of t^* for Greenland (Bougamont et al. 2005) are also applicable to Svalbard. Potential inaccuracies in parameters like t^* will introduce uncertainty in modelled albedo values, as it introduces compensating errors in calibrated parameters; in the case of t^*, compensating errors would arise in α_{fs} and P_{th}. However, the calibration procedure assures that, despite compensating errors, net biases in most relevant model output, e.g. melt, is minimized. More careful calibration of albedo parameters, including t^*, is planned for future work using a more extensive dataset of albedo measurements across Svalbard. As AWS data from only two ~~sites~~ regions in central and western Svalbard were used for energy balance model calibration, potential biases may arise for other areas in Svalbard. Regarding uncertainty in simulating subsurface conditions, it is worth noting that the recently implemented deep water percolation scheme (Sect. 3.1, Marchenko et al., 2017b) significantly reduces uncertainty in simulated firn temperatures compared to the earlier bucket scheme, which was found to underestimate rapid deep transport of water through piping. Furthermore, the comparison of simulated and observed bulk firn density shows good agreement (Sect. 3.3), and suggests that model-induced biases are small. We refrain from a detailed vertical comparison of simulated firn density profiles with observed firn core data, since previous work has shown the extremely local character of firn stratigraphy in Svalbard (Marchenko et al., 2017a), due to local interactions between stratigraphy and vertical water percolation. As in previous glacier basin-scale applications, we have applied substantial spin-up (25 years) to generate subsurface conditions at the start of the simulation, ~~which were consistent with the applied~~ using the climate forcing during 1957−1982. Obviously, this generates some uncertainty as the 1957−1982 may differ from the actual climate conditions in the decades prior to 1957. As discussed in Van Pelt and Kohler (2015), the impacts of perturbing temperature and precipitation during initialization on simulated climatic mass balance are typically only significant in the first few years of the simulation; impacts on simulated firn air content were found to be present even after 20 years into the simulation, which is, however, likely to be less significant in this study given the relatively shallow depth of the vertical domain of $<$20 m.

5 Conclusions

We present a model dataset of climatic mass balance, snow conditions and runoff for all of Svalbard for the period 1957−2018. Output with a 3-hourly temporal and 1×1-km spatial resolution is generated with a coupled surface energy balance − snow/firn/soil model. The model is forced with downscaled regional climate model fields and applied to both glacier-covered and land areas. In situ observational data from mass balance stakes, weather stations and shallow cores are used for model calibration and/or validation of the results. Based on the model output we analyze spatial variability and trends of climatic mass balance, equilibrium line altitude, glacier subsurface conditions, refreezing, seasonal snow season length and runoff.

We find an area-averaged positive CMB (+0.09 m w.e. a^{-1}), and a significant negative longterm trend (−0.06 m w.e. a^{-1} $decade^{-1}$) over the simulation period. The negative CMB trend has caused the ELA to increase (+17 m $decade^{-1}$) and the AAR to decrease (−0.04 $decade^{-1}$) markedly. These trends are significant for all of Svalbard, except for the most northern regions. Retreat of the ELA causes a significant reduction of mean firn air content (−0.09 m $decade^{-1}$), with the most pronounced changes (down to −0.6 m $decade^{-1}$) in ablation areas that were recently exposed by the retreating ELA. These new ablation zones also experience a strong decrease in temperature at 14 m depth (down to $-1.5\ ^{o}$C $decade^{-1}$), while the remainder of the ablation zones show a general warming trend. All high-altitude accumulation zones are found to exhibit temperate deep firn conditions, suggesting the potential for wide-spread presence of firn aquifers across Svalbard. We find average refreezing rates of 0.24 m w.e. a^{-1}, showing pronounced negative trends for both glacier-covered areas (−0.007 m w.e. a^{-1} $decade^{-1}$) and land areas (−0.008 m w.e. a^{-1} $decade^{-1}$). Increased precipitation and melt cause the date of disappearance of seasonal snow packs to remain stable throughout the simulation period, while increased autumn temperatures induce a significant increase in the date of seasonal snow onset (+1.4 days $decade^{-1}$). The average total runoff for Svalbard (44.9 Gt a^{-1}) is dominated by runoff from glaciers (34.3 Gt a^{-1}) rather than runoff from land (10.6 Gt a^{-1}). A strong positive runoff trend applies to glacier runoff (+3.7 Gt a^{-1} $decade^{-1}$), while runoff from land remained nearly stable (+0.2 Gt a^{-1} $decade^{-1}$), causing an increase in the relative contribution of glacier discharge to total runoff from 70 to 80% over the simulation period.

Data availability. The digital elevation model can be accessed at https://doi.org/10.21334/npolar.2014.dce53a47 (Norwegian Polar Institute, 2014). The glacier and land mask were constructed from glacier outlines, which are available at https://doi.org/10.21334/npolar.2013.89f430f8 (König et al., 2013). The model output behind the presented figures of air temperature, precipitation, CMB, ELA, runoff, refreezing, T_{14}, P_{14}, snow onset and disappearance dates are available in the following repository: https://doi.org/10.6084/m9.figshare.7836530.v1 (Van Pelt et al., 2019). The full model dataset, of which only a selection is presented here, contains data with a 3-hourly temporal resolution and for an extended set of variables; an overview of the readily available data can be found at http://www.wardvanpelt.com/model_output.txt. Glacier-wide mass balances for KNG, HBR, HDF, MLB and ABB are available in the database of the World Glacier Monitoring Service (WGMS; https://wgms.ch/). Meteorological time-series for Ny-Ålesund and Longyearbyen are accessible through the eKlima portal (Norwegian Meteorological Institute; http://eklima.met.no/). The Kongsvegen AWS time-series are also accessible at https://data.npolar.no/dataset/5dc31930-0922-4483-a1df-6f48af9e371b (Kohler et al., 2017). Unrestricted access to the HIRLAM regional climate model data, point stake

mass balance data, and the remaining AWS time-series is provided upon request by contacting the institutes that collected/generated the data (see Sect. 2).

Author contributions. The research idea was conceptualized by WvP, who also performed the main analysis. VP, RP, SM, JK, BL, JOH, TD, CR, TVS and WvP contributed to observational data collection and/or processing. WvP developed the model with support from SM. WvP wrote the manuscript with contributions from all co-authors.

Competing interests. The authors declare that they have no conflict of interest.

Acknowledgements. This work was performed with funding support from the Swedish Research Council (VR), Stiftelsen Ymer-80, Svalbard Integrated Arctic Earth Observing System (SIOS), Uppsala University (Finn Malmgren's stipend), the Norwegian Research Council (TIGRIF project), the Polish-Norwegian Research Programme GLAERE, and the Norwegian Polar Institute (TW-ICE project). We thank the Norwegian Meteorological Institute for providing access to the HIRLAM regional climate model output. We are further grateful to all the people that assisted with stake mass balance, AWS, and shallow-core measurements on glaciers in Svalbard over the years.

References

Aas, K. S., Dunse, T., Collier, E., Schuler, T. V., Berntsen, T. K., Kohler, J., and Luks, B.: The climatic mass balance of Svalbard glaciers: A 10-year simulation with a coupled atmosphere-glacier mass balance model, Cryosphere, https://doi.org/10.5194/tc-10-1089-2016, 2016.

AMAP: Snow, water, ice and permafrost in the Arctic (SWIPA), Arctic Monitoring and Assessment Programme (AMAP), Oslo, Norway, 2017.

Beaudon, E., Moore, J. C., Martma, T., Pohjola, V. A., Van de Wal, R. S., Kohler, J., and Isaksson, E.: Lomonosovfonna and Holtedahlfonna ice cores reveal east–west disparities of the Spitsbergen environment since AD 1700, Journal of Glaciology, 59, 1069–1083, https://doi.org/10.3189/2013JoG12J203, 2013.

Bevan, S. L., Luckman, A., Hubbard, B., Kulessa, B., Ashmore, D., Kuipers Munneke, P., O'Leary, M., Booth, A., Sevestre, H., and McGrath, D.: Centuries of intense surface melt on Larsen C Ice Shelf, The Cryosphere, 11, 2743–2753, https://doi.org/10.5194/tc-11-2743-2017, 2017.

Bezeau, P., Sharp, M., Burgess, D., and Gascon, G.: Firn profile changes in response to extreme 21st-century melting at Devon Ice Cap, Nunavut, Canada, Journal of Glaciology, 59, 981–991, https://doi.org/10.3189/2013JoG12J208, 2013.

Bintanja, R. and Andry, O.: Towards a rain-dominated Arctic, Nature Climate Change, https://doi.org/10.1038/nclimate3240, 2017.

Bintanja, R. and Selten, F. M.: Future increases in Arctic precipitation linked to local evaporation and sea-ice retreat, Nature, https://doi.org/10.1038/nature13259, 2014.

Bintanja, R. and Van Der Linden, E. C.: The changing seasonal climate in the Arctic, Scientific Reports, https://doi.org/10.1038/srep01556, 2013.

Björnsson, H., Gjessing, Y., Hamran, S.-E., Hagen, J. O., LiestøL, O., Pálsson, F., and Erlingsson, B.: The thermal regime of sub-polar glaciers mapped by multi-frequency radio-echo sounding, Journal of Glaciology, 42, 23–32, https://doi.org/10.3189/S0022143000030495, 1996.

Blaszczyk, M., Jania, J. a., and Hagen, J. O.: Tidewater glaciers of Svalbard: Recent changes and estimates of calving fluxes, Polish Polar Research, 30, 85–142, 2009.

Bougamont, M., Bamber, J. L., and Greuell, W.: A surface mass balance model for the Greenland Ice Sheet, Journal of Geophysical Research: Earth Surface, 110, n/a–n/a, https://doi.org/10.1029/2005JF000348, 2005.

Christianson, K., Kohler, J., Alley, R. B., Nuth, C., and van Pelt, W. J. J.: Dynamic perennial firn aquifer on an Arctic glacier, Geophysical Research Letters, 42, 1418–1426, https://doi.org/10.1002/2014GL062806, 2015.

Cogley, J. G., Hock, R., Rasmussen, L. A., Arendt, A. A., Bauder, A., Braithwaite, R. J., Jansson, M., Kaser, G., Möller, M., Nicholson, L., and Zemp, M.: Glossary of glacier mass balance, Tech. rep., UNESCO-IHP, Paris, https://doi.org/10.2172/776739, 2011.

Cox, C., Humphrey, N., and Harper, J.: Quantifying meltwater refreezing along a transect of sites on the Greenland ice sheet, The Cryosphere, 9, 691–701, https://doi.org/10.5194/tc-9-691-2015, 2015.

Day, J. J., Bamber, J. L., Valdes, P. J., and Kohler, J.: The impact of a seasonally ice free Arctic Ocean on the temperature, precipitation and surface mass balance of Svalbard, Cryosphere, https://doi.org/10.5194/tc-6-35-2012, 2012.

Dee, D. P., Uppala, S. M., Simmons, A. J., Berrisford, P., Poli, P., Kobayashi, S., Andrae, U., Balmaseda, M. A., Balsamo, G., Bauer, P., Bechtold, P., Beljaars, A. C., van de Berg, L., Bidlot, J., Bormann, N., Delsol, C., Dragani, R., Fuentes, M., Geer, A. J., Haimberger, L., Healy, S. B., Hersbach, H., Hólm, E. V., Isaksen, L., Kållberg, P., Köhler, M., Matricardi, M., Mcnally, A. P., Monge-Sanz, B. M., Morcrette, J. J., Park, B. K., Peubey, C., de Rosnay, P., Tavolato, C., Thépaut, J. N., and Vitart, F.: The ERA-Interim reanalysis: Configuration

and performance of the data assimilation system, Quarterly Journal of the Royal Meteorological Society, https://doi.org/10.1002/qj.828, 2011.

Deschamps-Berger, C., Nuth, C., Van Pelt, W. J. J., Berthier, E., Kohler, J., and Altena, B.: Closing the mass budget of a tidewater glacier: the example of Kronebreen, Svalbard, Journal of Glaciology, pp. 1–13, https://doi.org/10.1017/jog.2018.98, 2019.

Divine, D. V. and Dick, C.: Historical variability of sea ice edge position in the Nordic Seas, Journal of Geophysical Research: Oceans, https://doi.org/10.1029/2004JC002851, 2006.

Elsberg, D. H., Harrison, W. D., Echelmeyer, K. A., and Krimmel, R. M.: Quantifying the effects of climate and surface change on glacier mass balance, Journal of Glaciology, 47, 649–658, https://doi.org/10.3189/172756501781831783, 2001.

Førland, E. J. and Hanssen-Bauer, I.: Increased precipitation in the Norwegian Arctic: True or false?, Climatic Change, https://doi.org/10.1023/A:1005613304674, 2000.

Førland, E. J., Benestad, R., Hanssen-Bauer, I., Haugen, J. E., and Skaugen, T. E.: Temperature and precipitation development at Svalbard 1900–2100, Advances in Meteorology, https://doi.org/10.1155/2011/893790, 2011.

Fürst, J. J., Navarro, F., Gillet-Chaulet, F., Huss, M., Moholdt, G., Fettweis, X., Lang, C., Seehaus, T., Ai, S., Benham, T. J., Benn, D. I., Björnsson, H., Dowdeswell, J. A., Grabiec, M., Kohler, J., Lavrentiev, I., Lindbäck, K., Melvold, K., Pettersson, R., Rippin, D., Saintenoy, A., Sánchez-Gámez, P., Schuler, T. V., Sevestre, H., Vasilenko, E., and Braun, M. H.: The Ice-Free Topography of Svalbard, Geophysical Research Letters, 45, 11,760–11,769, https://doi.org/10.1029/2018GL079734, 2018.

Grabiec, M., Puczko, D., Budzik, T., and Gajek, G.: Snow distribution patterns on Svalbard glaciers derived from radio-echo soundings, Polish Polar Research, 32, 393–421, https://doi.org/10.2478/v10183-011-0026-4, 2011.

Grabiec, M., Jania, J., Puczko, D., Kolondra, L., and Budzik, T.: Surface and bed morphology of Hansbreen, a tidewater glacier in Spitsbergen, Polish Polar Research, 33, 111–138, https://doi.org/10.2478/v10183-012-0010-7, 2012.

Hagen, J., Melvold, K., Eiken, T., Isaksson, E., and Lefauconnier, B.: Mass balance methods on Kongsvegen, Svalbard, Geografiska Annaler, Series A: Physical Geography, 81, 593–601, https://doi.org/10.1111/1468-0459.00087, 1999.

Hagen, J. O., Kohler, J., Melvold, K., and Winther, J. G.: Glaciers in Svalbard: Mass balance, runoff and freshwater flux, Polar Research, https://doi.org/10.1016/0022-460X(87)90195-7, 2003.

Hansen, B. B., Aanes, R., Herfindal, I., Kohler, J., Sæther, B. E., and Oli, M. K.: Climate, icing, and wild arctic reindeer: Past relationships and future prospects, Ecology, https://doi.org/10.1890/11-0095.1, 2011.

Hansen, B. B., Isaksen, K., Benestad, R. E., Kohler, J., Pedersen, Å., Loe, L. E., Coulson, S. J., Larsen, J. O., and Varpe, Ø.: Warmer and wetter winters: Characteristics and implications of an extreme weather event in the High Arctic, Environmental Research Letters, https://doi.org/10.1088/1748-9326/9/11/114021, 2014.

Hanssen-Bauer, I. and Førland, E. J.: Long-term trends in precipitation and temperature in the Norwegian Arctic: Can they be explained by changes in atmospheric circulation patterns?, Climate Research, https://doi.org/10.3354/cr010143, 1998.

How, P., Benn, D. I., Hulton, N. R. J., Hubbard, B., Luckman, A., Sevestre, H., van Pelt, W. J. J., Lindbäck, K., Kohler, J., and Boot, W.: Rapidly changing subglacial hydrological pathways at a tidewater glacier revealed through simultaneous observations of water pressure, supraglacial lakes, meltwater plumes and surface velocities, The Cryosphere, 11, 2691–2710, https://doi.org/10.5194/tc-11-2691-2017, 2017.

Hubbard, B., Luckman, A., Ashmore, D. W., Bevan, S., Kulessa, B., Kuipers Munneke, P., Philippe, M., Jansen, D., Booth, A., Sevestre, H., Tison, J.-L., O'Leary, M., and Rutt, I.: Massive subsurface ice formed by refreezing of ice-shelf melt ponds, Nature Communications, 7, 11 897, https://doi.org/10.1038/ncomms11897, 2016.

IPCC: Summary for policymakers, in: Climate Change 2013 - The Physical Science Basis, edited by Intergovernmental Panel on Climate Change, Cambridge University Press, Cambridge, https://doi.org/10.1017/CBO9781107415324.004, 2014.

Jaedicke, C. and Gauer, P.: The influence of drifting snow on the location of glaciers on western Spitsbergen, Svalbard, Annals of Glaciology, 42, 237–242, https://doi.org/10.3189/172756405781812628, 2005.

Karner, F., Obleitner, F., Krismer, T., Kohler, J., and Greuell, W.: A decade of energy and mass balance investigations on the glacier Kongsvegen, Svalbard, Journal of Geophysical Research: Atmospheres, 118, 3986–4000, https://doi.org/10.1029/2012JD018342, 2013.

Kohler, J. and Aanes, R.: Effect of winter snow and ground-icing on a Svalbard reindeer population: results of a simple snowpack model, Arctic, Antarctic, and Alpine Research, https://doi.org/10.1657/1523-0430(2004)036[0333:EOWSAG]2.0.CO;2, 2009.

Kohler, J., James, T. D., Murray, T., Nuth, C., Brandt, O., Barrand, N. E., Aas, H. F., and Luckman, A.: Acceleration in thinning rate on western Svalbard glaciers, Geophysical Research Letters, 34, L18 502, https://doi.org/10.1029/2007GL030681, 2007.

Kohler, J., Hudson, S., and Obleitner, F.: Automatic weather station data from Kongsvegen, Ny-Ålesund [Data set], Norwegian Polar Institute, https://doi.org/10.21334/npolar.2017.5dc31930, 2017.

König, M., Kohler, J., and Nuth, C.: Glacier Area Outlines - Svalbard [Data set], Norwegian Polar Institute, https://doi.org/10.21334/npolar.2013.89f430f8, 2013.

König, M., Nuth, C., Kohler, J., Moholdt, G., and Pettersen, R.: A digital glacier database for Svalbard, in: Global Land Ice Measurements from Space, Springer Praxis Books, Berlin, Heidelberg, https://doi.org/10.1007/978-3-540-79818-7_10, 2014.

Kuipers Munneke, P., Ligtenberg, S. R. M., van den Broeke, M. R., van Angelen, J. H., and Forster, R. R.: Explaining the presence of perennial liquid water bodies in the firn of the Greenland Ice Sheet, Geophysical Research Letters, 41, 476–483, https://doi.org/10.1002/2013GL058389, 2014.

Lang, C., Fettweis, X., and Erpicum, M.: Stable climate and surface mass balance in Svalbard over 1979-2013 despite the Arctic warming, Cryosphere, https://doi.org/10.5194/tc-9-83-2015, 2015.

Ligtenberg, S. R. M., Helsen, M. M., and van den Broeke, M. R.: An improved semi-empirical model for the densification of Antarctic firn, The Cryosphere, 5, 809–819, https://doi.org/10.5194/tc-5-809-2011, 2011.

Machguth, H., MacFerrin, M., van As, D., Box, J. E., Charalampidis, C., Colgan, W., Fausto, R. S., Meijer, H. A. J., Mosley-Thompson, E., and van de Wal, R. S. W.: Greenland meltwater storage in firn limited by near-surface ice formation, Nature Climate Change, 6, 390–393, https://doi.org/10.1038/nclimate2899, 2016.

Marchenko, S., Pohjola, V. A., Pettersson, R., Van Pelt, W. J. J., Vega, C. P., Machguth, H., Boggild, C. E., and Isaksson, E.: A plot-scale study of firn stratigraphy at Lomonosovfonna, Svalbard, using ice cores, borehole video and GPR surveys in 2012–14, Journal of Glaciology, 63, 67–78, https://doi.org/10.1017/jog.2016.118, 2017a.

Marchenko, S., Van Pelt, W. J. J., Claremar, B., Pohjola, V., Pettersson, R., Machguth, H., and Reijmer, C.: Parameterizing deep water percolation improves subsurface temperature simulations by a multilayer firn model, Frontiers in Earth Science, 5, https://doi.org/10.3389/feart.2017.00016, 2017b.

Moholdt, G., Nuth, C., Hagen, J. O., and Kohler, J.: Recent elevation changes of Svalbard glaciers derived from ICESat laser altimetry, Remote Sensing of Environment, https://doi.org/10.1016/j.rse.2010.06.008, 2010.

Möller, M. and Kohler, J.: Differing climatic mass balance evolution across Svalbard glacier regions over 1900–2010, Frontiers in Earth Science, 6, https://doi.org/10.3389/feart.2018.00128, 2018.

Möller, M., Finkelnburg, R., Braun, M., Scherer, D., and Schneider, C.: Variability of the climatic mass balance of Vestfonna ice cap, northeastern Svalbard, 1979-2011, Annals of Glaciology, https://doi.org/10.3189/2013AoG63A407, 2013.

Möller, M., Obleitner, F., Reijmer, C. H., Pohjola, V. A., Głowacki, P., and Kohler, J.: Adjustment of regional climate model output for modeling the climatic mass balance of all glaciers on Svalbard, Journal of Geophysical Research: Atmospheres, 121, 5411–5429, https://doi.org/10.1002/2015JD024380, 2016.

Noël, B., Van de Berg, W. J., Lhermitte, S., Wouters, B., Machguth, H., Howat, I., Citterio, M., Moholdt, G., Lenaerts, J. T. M., and van den Broeke, M. R.: A tipping point in refreezing accelerates mass loss of Greenland's glaciers and ice caps, Nature Communications, 8, 14 730, https://doi.org/10.1038/ncomms14730, 2017.

Noël, B., Van de Berg, W. J., Lhermitte, S., Wouters, B., Schaffer, N., and Van den Broeke, M. R.: Six Decades of Glacial Mass Loss in the Canadian Arctic Archipelago, Journal of Geophysical Research: Earth Surface, 123, 1430–1449, https://doi.org/10.1029/2017JF004304, 2018.

Nordli, Ø., Przybylak, R., Ogilvie, A. E., and Isaksen, K.: Long-term temperature trends and variability on Spitsbergen: The extended Svalbard airport temperature series, 1898-2012, Polar Research, https://doi.org/10.3402/polar.v33.21349, 2014.

Norwegian Polar Institute: Terrengmodell Svalbard (S0 Terrengmodell) [Data set], Norwegian Polar Institute, https://doi.org/10.21334/npolar.2014.dce53a47, 2014.

Nuth, C., Moholdt, G., Kohler, J., Hagen, J. O., and Kääb, A.: Svalbard glacier elevation changes and contribution to sea level rise, Journal of Geophysical Research: Earth Surface, 115, https://doi.org/10.1029/2008JF001223, 2010.

Nuth, C., Schuler, T. V., Kohler, J., Altena, B., and Hagen, J. O.: Estimating the long-term calving flux of Kronebreen, Svalbard from geodetic elevation changes and mass-balance modelling, Journal of Glaciology, https://doi.org/10.3189/2012JoG11J036, 2012.

Nuth, C., Kohler, J., König, M., Von Deschwanden, A., Hagen, J. O., Kääb, A., Moholdt, G., and Pettersson, R.: Decadal changes from a multi-temporal glacier inventory of Svalbard, Cryosphere, https://doi.org/10.5194/tc-7-1603-2013, 2013.

Oerlemans, J. and Grisogono, B.: Glacier winds and parameterisation of the related surface heat fluxes, Tellus A: Dynamic Meteorology and Oceanography, 54, 440–452, https://doi.org/10.3402/tellusa.v54i5.12164, 2002.

Oerlemans, J. and Knap, W. H.: A 1 year record of global radiation and albedo in the ablation zone of Morteratschgletscher, Switzerland, Journal of Glaciology, 44, 231–238, https://doi.org/10.3189/S0022143000002574, 1998.

Østby, T. I., Vikhamar Schuler, T., Ove Hagen, J., Hock, R., Kohler, J., and Reijmer, C. H.: Diagnosing the decline in climatic mass balance of glaciers in Svalbard over 1957-2014, Cryosphere, https://doi.org/10.5194/tc-11-191-2017, 2017.

Pettersson, R.: Dynamics of the cold surface layer of polythermal Storglaciären, Sweden, Ph.D. thesis, Stockholm University, 2004.

Pohjola, V. A., Martma, T. A., Meijer, H. A. J., Moore, J. C., Isaksson, E., Vaikmäe, R., and van de Wal, R. S.: Reconstruction of three centuries of annual accumulation rates based on the record of stable isotopes of water from Lomonosovfonna, Svalbard, Annals of Glaciology, 35, 57–62, https://doi.org/10.3189/172756402781816753, 2002.

Pramanik, A., Van Pelt, W. J. J., Kohler, J., and Schuler, T. V.: Simulating climatic mass balance, seasonal snow development and associated freshwater runoff in the Kongsfjord basin, Svalbard (1980–2016), Journal of Glaciology, 64, 943–956, https://doi.org/10.1017/jog.2018.80, 2018.

Reistad, M., Breivik, Ø., Haakenstad, H., Aarnes, O. J., Furevik, B. R., and Bidlot, J. R.: A high-resolution hindcast of wind and waves for the North Sea, the Norwegian Sea, and the Barents Sea, Journal of Geophysical Research: Oceans, https://doi.org/10.1029/2010JC006402, 2011.

Rye, C. J., Willis, I. C., Arnold, N. S., and Kohler, J.: On the need for automated multiobjective optimization and uncertainty estimation of glacier mass balance models, Journal of Geophysical Research: Earth Surface, 117, https://doi.org/10.1029/2011JF002184, 2012.

Schuler, T. V., Dunse, T., Østby, T. I., and Hagen, J. O.: Meteorological conditions on an Arctic ice cap-8 years of automatic weather station data from Austfonna, Svalbard, International Journal of Climatology, 34, 2047–2058, https://doi.org/10.1002/joc.3821, 2014.

Serreze, M. C. and Barry, R. G.: Processes and impacts of Arctic amplification: A research synthesis, Global and Planetary Change, https://doi.org/10.1016/j.gloplacha.2011.03.004, 2011.

Uppala, S. M., Kållberg, P. W., Simmons, A. J., Andrae, U., Bechtold, V. D. C., Fiorino, M., Gibson, J. K., Haseler, J., Hernandez, A., Kelly, G. A., Li, X., Onogi, K., Saarinen, S., Sokka, N., Allan, R. P., Andersson, E., Arpe, K., Balmaseda, M. A., Beljaars, A. C. M., Berg, L. V. D., Bidlot, J., Bormann, N., Caires, S., Chevallier, F., Dethof, A., Dragosavac, M., Fisher, M., Fuentes, M., Hagemann, S., Hólm, E., Hoskins, B. J., Isaksen, L., Janssen, P. A. E. M., Jenne, R., Mcnally, A. P., Mahfouf, J.-F., Morcrette, J.-J., Rayner, N. A., Saunders, R. W., Simon, P., Sterl, A., Trenberth, K. E., Untch, A., Vasiljevic, D., Viterbo, P., and Woollen, J.: The ERA-40 re-analysis, Quarterly Journal of the Royal Meteorological Society, 131, 2961–3012, https://doi.org/10.1256/qj.04.176, 2005.

Vallot, D., Pettersson, R., Luckman, A., Benn, D. I., Zwinger, T., Van Pelt, W. J. J., Kohler, J., Schäfer, M., Claremar, B., and Hulton, N. R.: Basal dynamics of Kronebreen, a fast-flowing tidewater glacier in Svalbard: non-local spatio-temporal response to water input, Journal of Glaciology, 63, 1012–1024, https://doi.org/10.1017/jog.2017.69, 2017.

Van de Wal, R. S., Mulvaney, R., Isaksson, E., Moore, J. C., Pinglot, J. F., Pohjola, V. A., and Thomassen, M. P. A.: Reconstruction of the historical temperature trend from measurements in a medium-length borehole on the Lomonosovfonna plateau, Svalbard, Annals of Glaciology, 35, 371–378, https://doi.org/10.3189/172756402781816979, 2002.

Van der Wel, L., Streurman, H., Isaksson, E., Helsen, M., Van de Wal, R., Martma, T., Pohjola, V., Moore, J., and Meijer, H.: Using high-resolution tritium profiles to quantify the effects of melt on two Spitsbergen ice cores, Journal of Glaciology, 57, 1087–1097, https://doi.org/10.3189/002214311798843368, 2011.

Van Pelt, W. J. J. and Kohler, J.: Modelling the long-term mass balance and firn evolution of glaciers around Kongsfjorden, Svalbard, Journal of Glaciology, https://doi.org/10.3189/2015JoG14J223, 2015.

Van Pelt, W. J. J., Oerlemans, J., Reijmer, C. H., Pohjola, V. A., Pettersson, R., and Van Angelen, J. H.: Simulating melt, runoff and refreezing on Nordenskiöldbreen, Svalbard, using a coupled snow and energy balance model, Cryosphere, https://doi.org/10.5194/tc-6-641-2012, 2012.

Van Pelt, W. J. J., Pettersson, R., Pohjola, V. A., Marchenko, S., Claremar, B., and Oerlemans, J.: Inverse estimation of snow accumulation along a radar transect on Nordenskiöldbreen, Svalbard, Journal of Geophysical Research: Earth Surface, https://doi.org/10.1002/2013JF003040, 2014.

Van Pelt, W. J. J., Kohler, J., Liston, G. E., Hagen, J. O., Luks, B., Reijmer, C. H., and Pohjola, V. A.: Multidecadal climate and seasonal snow conditions in Svalbard, Journal of Geophysical Research: Earth Surface, https://doi.org/10.1002/2016JF003999, 2016a.

Van Pelt, W. J. J., Pohjola, V. A., and Reijmer, C. H.: The changing impact of snow conditions and refreezing on the mass balance of an idealized Svalbard glacier, Frontiers in Earth Science, https://doi.org/10.3389/feart.2016.00102, 2016b.

Van Pelt, W. J. J., Pohjola, V. A., Pettersson, R., Ehwald, L. E., Reijmer, C. H., Boot, W., and Jakobs, C. L.: Dynamic response of a High Arctic glacier to melt and runoff variations, Geophysical Research Letters, 45, 4917–4926, https://doi.org/10.1029/2018GL077252, 2018.

Van Pelt, W. J. J., Pohjola, V. A., Pettersson, R., Marchenko, S., Kohler, J., Luks, B., Hagen, J. O., Schuler, T. V., Dunse, T., Noël, B., and Reijmer, C. H.: A long-term dataset of climatic mass balance, snow conditions and runoff in Svalbard (1957-2018) [Data set], https://doi.org/10.6084/m9.figshare.7836530.v1, 2019.

Vega, C. P., Pohjola, V. A., Beaudon, E., Claremar, B., Van Pelt, W. J. J., Pettersson, R., Isaksson, E., Martma, T., Schwikowski, M., and Bøggild, C. E.: A synthetic ice core approach to estimate ion relocation in an ice field site experiencing periodical melt: a case study on Lomonosovfonna, Svalbard, The Cryosphere, 10, 961–976, https://doi.org/10.5194/tc-10-961-2016, 2016.

Westermann, S., Boike, J., Langer, M., Schuler, T. V., and Etzelmüller, B.: Modeling the impact of wintertime rain events on the thermal regime of permafrost, The Cryosphere, 5, 945–959, https://doi.org/10.5194/tc-5-945-2011, 2011.

Winsvold, S. H., Kääb, A., Nuth, C., Andreassen, L. M., Van Pelt, W. J. J., and Schellenberger, T.: Using SAR satellite data time series for regional glacier mapping, The Cryosphere, 12, 867–890, https://doi.org/10.5194/tc-12-867-2018, 2018.

Winther, J. G., Bruland, O., Sand, K., Gerland, S., Marechal, D., Ivanov, B., Głowacki, P., and König, M.: Snow research in Svalbard - An overview, Polar Research, https://doi.org/10.1111/j.1751-8369.2003.tb00103.x, 2003.

Zhang, X., He, J., Zhang, J., Polyakov, I., Gerdes, R., Inoue, J., and Wu, P.: Enhanced poleward moisture transport and amplified northern high-latitude wetting trend, Nature Climate Change, https://doi.org/10.1038/nclimate1631, 2013.